Poly(allylamine)/tripolyphosphate nanocomplex coacervate as a NLRP3-dependent systemic adjuvant for vaccine development

Gastón P. Rizzo[1], Rodrigo C. Sanches[2], Camila Chavero[1], Daiana S. Bianchi[1], Eugenia Apuzzo[3], Santiago E. Herrera[4], Maximiliano L. Agazzi[5], M. Lorena Cortez[3], Waldemar A. Marmisollé[3], Irene A. Keitelman[6], Analía S. Trevani[6], Sergio C. Oliveira[2,7], Omar Azzaroni[3], Paola L. Smaldini[1†], Guillermo H. Docena[1†].*

[1]Instituto de Estudios Inmunológicos y Fisiopatológicos (IIFP), UNLP, CONICET, asociado a CIC PBA, Facultad de Ciencias Exactas, Departamento de Ciencias Biológicas, La Plata, Argentina (IIFP-UNLP-CONICET).

[2]Department of Biochemistry and Immunology, Institute of Biological Sciences, Federal University of Minas Gerais (ICB-UFMG).

[3]Instituto de Investigaciones Fisicoquímicas Teóricas y Aplicadas (INIFTA), (UNLP, CONICET), 1900 La Plata, Buenos Aires, Argentina.

[4]Instituto de Química de los Materiales, Ambiente y Energía (INQUIMAE), UBA, CONICET, Facultad de Ciencias Exactas y Naturales, Departamento de Química Inorgánica Analítica y Química Física. Buenos Aires, Argentina.

[5]Instituto para el Desarrollo Agroindustrial y de la Salud (IDAS), (UNRC, CONICET), Ruta Nacional 36 KM 601, 5800 Río Cuarto, Argentina.

[6]Laboratorio de Inmunidad Innata, Instituto de Medicina Experimental (IMEX), CONICET, Academia Nacional de Medicina, Buenos Aires, Argentina.

[7]Department of Immunology, Institute of Biomedical Sciences, University of São Paulo (USP)

[†]Shared senior authorship

***Corresponding author:** Paola L. Smaldini; paola.smaldini@gmail.com

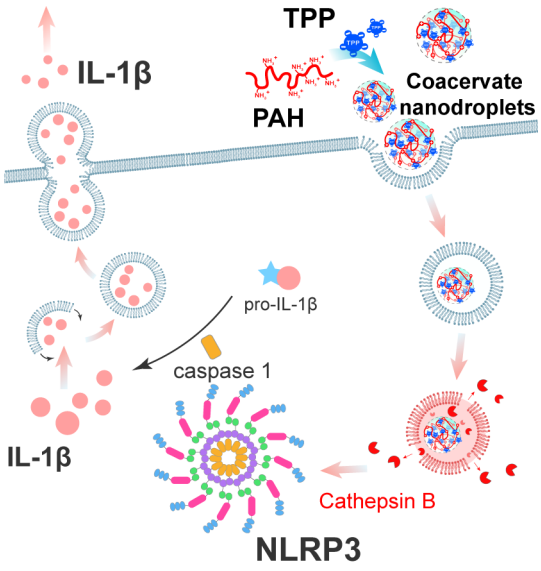

Graphical Abstract

ABSTRACT

Nanotechnology plays a crucial role in vaccine development. It allows the design of functional nanoparticles (NPs) that can act both as antigen carriers and as adjuvants to enhance the immune response. The present study aims to evaluate complex coacervate-like NPs composed of poly(allylamine hydrochloride) (PAH) and tripolyphosphate (TPP) as a safe vehicle and adjuvant for systemic vaccines. We investigated the activation of different antigen-presenting cells (APCs) with NPs and their adjuvanticity in Balbc/c and different KO mice that were intraperitoneally immunized with NP-OVA.

We found that NPs increased the expression of CD86 and MHCII and promoted the production and secretion of interleukin-1β (IL-1β) and IL-18 through the inflammasome NLRP3 when macrophages and dendritic cells were co-incubated with LPS and NPs. We evidenced an unconventional IL-1β release through the autophagosome pathway. The inhibition of autophagy with 3-methyladenine reduced the LPS/NPs-induced IL-1β secretion. Additionally, our findings showed that the systemic administration of mice with NP-OVA triggered a significant induction of serum OVA-specific IgG and IgG2a, an increased secretion of IFN-γ by spleen cells, and high frequencies of LT $CD4^{+}IFN\text{-}\gamma^{+}$ and LT $CD8^{+}IFN\text{-}\gamma^{+}$. Our findings show that NPs promoted the inflammasome activation of innate cells with Th1-dependent adjuvant properties, making them valuable for formulating novel preventive or therapeutic vaccines for infectious and non-infectious diseases.

Keywords: Coacervate, Nanoparticle, Adjuvant, Inflammasome, NLRP3, Systemic vaccines.

52 **INTRODUCTION**

53 Vaccines have prevented millions of deaths in the last decades (mainly in the pediatric
54 population), reduced medical care costs, and allowed us to coexist peacefully with
55 pathogens.[1] Protein antigen-based vaccines have emerged as attractive vaccine platforms as
56 they are safer than traditional vaccines.[2] However, they often generate a weak immune
57 response when administered alone.[3] To overcome this limitation, adjuvant agents are
58 included in the formulations to enhance protection by induction of robust and perdurable
59 immunity.[4] These adjuvants trigger antigen-presenting cells (APCs) to release pro-
60 inflammatory mediators and promote the clonal expansion of helper and cytotoxic T
61 lymphocytes (CTLs), which target and destroy pathogen-containing bacteria and viruses, and
62 tumor cells.[5,6]

63 Another limitation of protein subunit-based vaccines is that protein- or peptide-based
64 antigens can be degraded by enzymes.[7] Nanotechnology offers approaches for the design of
65 nanostructures that allow encapsulation, protection and delivery of antigens.[3,8,9] For instance,
66 nanoparticle-based vaccines were shown to be safe and effective for immune intervention in
67 COVID-19. [10–12] In addition, some nanosystems can enhance immune responses and function
68 as self-adjuvants.[13–15] Some nanoparticles have been designed to trigger innate immunity by
69 activating the multiprotein complex known as the inflammasome in antigen-presenting
70 cells.[16–18] The process of internalization has been attributed to the similarities in size and
71 morphological characteristics between nanoparticles and pathogens.[19,20]

72 Similar to the molecular patterns found in microorganisms (MAMPs and PAMPs) and signals
73 from tissue damage (DAMPs) that activate the immune response, nanoparticle-associated
74 molecular patterns (NAMPs) have been identified for non-pathogenic nanoparticles.[19,21]
75 NAMPs can interact with pattern recognition receptors on the surface or inside cells,

76 initiating inflammatory responses that activate immune cells.[22,23] Among these receptors,
77 NLRP3, primarily expressed in myeloid cells like macrophages and dendritic cells, plays a
78 key role in detecting NAMPs. When nanoparticles disrupt the lysosomal membrane, enzymes
79 such as cathepsin B are released, triggering the activation of the NLRP3 inflammasome.[24]
80 Upon activation of the inflammasome, the adaptor protein ASC assembles into large
81 aggregates, which recruit pro-caspase-1, leading to its activation. This process activates the
82 pro-inflammatory cytokines IL-1β and IL-18 and the pore-forming protein gasdermin-D.
83 Gasdermin-D pores facilitate the release of IL-1β and IL-18 while damaging the cell
84 membrane, leading to an inflammatory form of cell death known as pyroptosis.[25,26] However,
85 some cytokines can be released through non-lytic pathways, including exocytosis or vesicle
86 release, bypassing cell death.[27,28] For instance, multivesicular bodies (MVBs), loaded with
87 endosomes containing the cytokine, undergo lysis upon release into the extracellular
88 environment, releasing the soluble cytokine.[29,30] Additionally, alternative "non-canonical"
89 inflammasome activation pathways involving caspase-11 have also been identified.[31,32]
90 Several delivery systems have been widely explored as adjuvant/delivery platforms for
91 protein-based subunit vaccines, including liposomes, PLGA nanoparticles, micelles, and
92 lipid–polymer hybrid nanosystems.[33–37] Coacervation-like nanoplatforms based on ionic
93 coacervation of polyamines (such as polyethyleneimine, chitosan, and polylysine) have
94 demonstrated attractive properties as adjuvants.[38–40] In general, coacervate-based
95 nanoformulations have been designed to exhibit a positive surface charge as APCs more
96 easily take them up with a negative surface charge.[7,41] However, cationic systems usually
97 present cytotoxicity due to their interaction with negatively charged biological membranes,
98 which can impair cellular activity, such as membrane disruption.[42,43] We recently reported
99 anionic coacervate nanoparticles (size ~200 nm and zeta potential ~ -30 mV) produced

100 through the direct and fully aqueous assembly of polyallylamine (PAH) with the
101 tripolyphosphate anion (TPP), which exhibited long-term stability and ability to encapsulate
102 proteins.[44] Additionally, these nanostructures were non-toxic and demonstrated efficient
103 uptake by APCs, such as macrophages.[45]
104 Given the promising properties of PAH/TPP nanoparticles, here we explored their potential
105 as adjuvants to enhance immune system activation. Encapsulating an immunogen in this
106 system may trigger the immune system by activating innate cells and endowing them with
107 migratory capacity toward lymph nodes, where they can promote the activation of naïve B
108 and T cells. This approach could make these nanoparticles suitable for vaccine formulation.
109 Furthermore, activating these innate cells can lead to the production of cytokines and
110 chemokines, along with the increased expression of key surface markers such as CD80,
111 CD86, and MHCII. These changes transform the cells into potent APCs, enhancing their
112 ability to activate T lymphocytes.[46–48] In this work, we found that dendritic cells and
113 macrophages undergo activation upon nanoparticle uptake and promotion of Th1-dependent
114 adaptive immunity. The release of IL-1β and IL-18 through the NLRP3 activation (Figure
115 1A) triggered the secretion of IFN-γ with the induction of specific IgG antibodies (Figure
116 1B). Collectively, our findings indicated this PAH/TPP coacervate nanoformulation could
117 serve a dual purpose: acting as a safe vehicle for antigen stabilization and delivery while also
118 amplifying the immune response as nano adjuvants in the development of vaccine platforms.
119

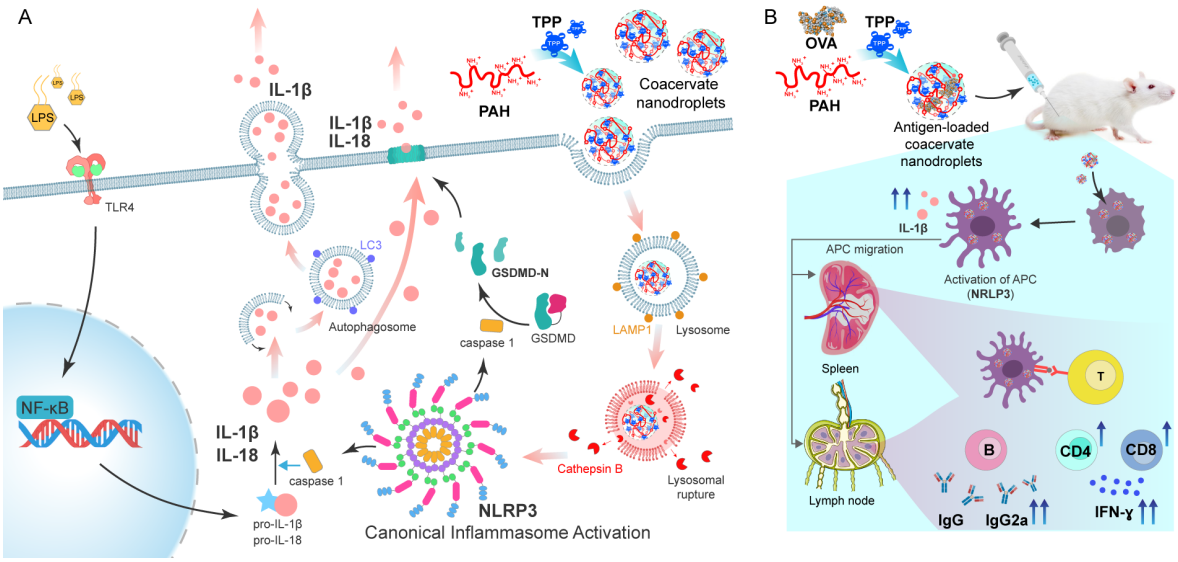

Figure 1. **Mechanisms of NP-induced immune activation. (A)** Schematic representation of NP uptake and NLRP3 inflammasome activation in phagocytic cells. Following NP internalization by phagocytosis, NPs are trafficked to lysosomes, where lysosomal membrane destabilization leads to the release of cathepsin B. Cathepsin B triggers the NLRP3 inflammasome pathway, leading to the activation of caspase-1, following the cleavage of Gasdermin D, and maturation of pro-IL-1β and pro-IL-18 for secretion. For the canonical inflammasome pathway, cells require an initial signal through Toll-like receptor to produce the pro-cytokines. Notably, the absence of pyroptosis, IL-1β can be released via the non-canonical autophagy pathway. **(B)** Systemic inoculation scheme with NP-OVA, leading to activation of phagocytic cells and subsequent migration to secondary lymphoid nodes, where they activate CD4+ and CD8+ T cells that produce IFN-γ and promote the activation of B cells for production of IgG and IgG2a antibodies.

RESULTS

Nanoparticle preparation and characterization

The interaction of polyamines with negatively charged multivalent small molecules was thoroughly studied over the past years. When mixing these components in an aqueous solution, a phase condensation takes place, leading to the formation of asymmetric polyelectrolyte complexes in which both intrinsic and extrinsic ion pairs are present between the long-chain polycation and short-chain polyanions.[49,50] At charge-matching conditions

(i.e. when the total amount of negative charges is equal to the total amount of positive charges), the mixing of polyamines with polyphosphates usually undergo macroscopic phases that go from insoluble solids (heavily crosslinked polyelectrolyte complexes) to polyelectrolyte-rich immiscible liquids (complex coacervates) depending on the pH and monovalent salt concentration. Recently, we reported the formation of an asymmetric coacervate composed of PAH (long-chain polyelectrolyte block) and TPP (small multivalent molecule).[44] We showed that if the mixture is prepared under highly non-stoichiometric conditions and in the absence of added monovalent salts, it is possible to prevent the colloidal dispersion of coacervate droplets from collapsing into a macroscopic liquid phase, as typically occurs when symmetric coacervates are prepared under stoichiometric conditions. Figure 2A shows a simplified scheme of the preparation of a dispersion of nanometric-sized coacervate droplets formed by PAH chains ionically crosslinked by TPP anions (nanocomplexes). From here on, for simplicity, we will refer to these as nanoparticles (NPs).

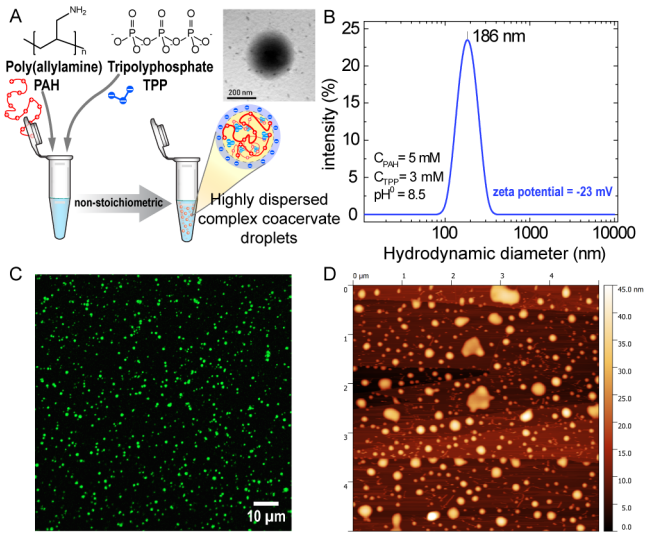

Figure 2. **NP characterization**. (A) PAH/TPP NP synthesis scheme. 5 mM PAH (monomer concentration) and 3 mM TPP are mixed in aqueous solution to obtain a highly stable colloidal dispersion of (asymmetric) coacervate droplets stabilized by electrostatic repulsions. Inset shows a TEM image of a single PAH/TPP NP.

155 (B) DLS measurements showing a single size distribution (particle hydrodynamic diameter) centered at 186
156 nm. (C) Confocal microscopy image of a cover slip after being in contact over 2 min with a PAH*/TPP NP
157 dispersion. (D) AFM (tapping mode) topography image of an HOPG flat substrate after being in contact over 2
158 min with a PAH/TPP NP dispersion.

159 Through dynamic light scattering (DLS) measurements, we detected a single distribution of
160 particle sizes with a mean hydrodynamic diameter near 200 nm (Figure 2B and TEM) and a
161 ζ-potential of -23 mV. Also, NPs were shown to remain stable in colloidal dispersion for
162 more than 9 months after storing in a closed vessel,[44] a key feature that can be explained by
163 the negative surface charge of the NPs thanks to the excess of negative charges coming from
164 the TPP anions. Also, we demonstrated that using a ratio of concentrations C_{TPP}/C_{PAH}=0.6,
165 the excess of negative charges forces almost all of PAH chains (~95%) to be ionically
166 crosslinked, which means that no free PAH remains in solution phase.[44] Using FITC-labeled
167 PAH (PAH*), we observed that PAH*/TPP NPs exhibit a homogeneous size distribution
168 when observed under confocal microscopy (Figure 2C). Finally, atomic force microscopy
169 (AFM) measurements showed that, upon contact with a flat surface such as HOPG, NPs tend
170 to deform by expanding in diameter and compressing in height, demonstrating their viscous
171 nature (Figure 2D).

172

173 *Nanoparticle internalization triggers activation in phagocytic cells.*

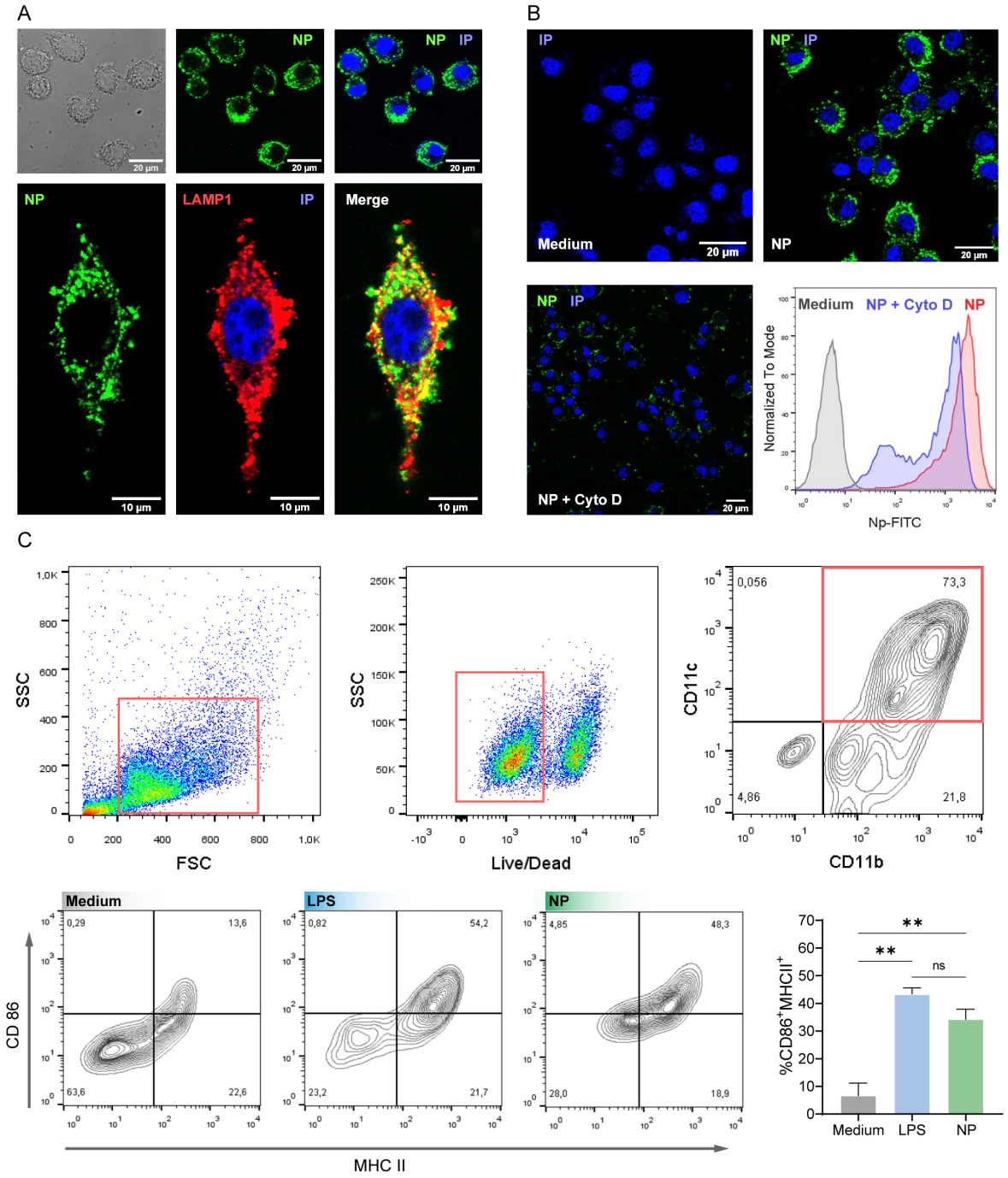

Figure 3. **Cell uptake of NP and activation. (A)** NP-FITC internalized by J774 and colocalized with the late endosome marker LAMP-1 by confocal microscopy after 4h stimulation. **(B)** Inhibition of phagocytosis of NP-FITC with cytochalasin D in BMDM by confocal microscopy and flow cytometry. **(C)** Surface expression of CD86 and MHCII in BMDC ($CD11b^{+}CD11c^{+}$) by flow cytometry. All experiments were performed in triplicate

179 and data are expressed as mean±SEM. P-value was determined by ordinary one-way ANOVA *P<0,05;
180 **P<0,01.

181 To study the interaction of PAH/TPP NPs with cells, we exposed the murine J774
182 macrophages to NPs. We observed the internalization and cellular distribution of fluorescent
183 NPs by confocal microscopy after 4h of incubation. Furthermore, we did not detect any
184 internalization of the polymer PAH-FITC (without TPP) in macrophages (Figure S1). We
185 observed that nanoparticles were well-dispersed into cytoplasmic vesicles (fluorescent
186 granules) and the cytosol (diffuse fluorescence) (Figure 3A). Then, we analyzed the co-
187 localization of the NP-FITC with LAMP1 to define the NP localization in vesicles. As it can
188 be observed in Figure 3A, NPs were distributed between $LAMP1^{+}$- and $LAMP1^{-}$-vesicles,
189 likely late and early endosomes (yellow and green vesicles, respectively). The incubation of
190 cells along with the phagocytosis inhibitor cytochalasin D (Cyto D) confirmed that the
191 internalization of NP was dependent on phagocytosis. Additionally, we detected lower
192 fluorescence by flow cytometry in macrophages $F4/80^{+}$ $CD11b^{+}$ (Figure S1C) incubated with
193 Cyto D than in cells exposed to NP-FITC (Figure 3B). Next, bone marrow-derived dendritic
194 cells (BMDC) were exposed to NP or LPS and we analyzed the surface expression of Class
195 II MHC and CD86 as cell activation markers (Figure 3C). We found that BMDC expressed
196 significantly higher levels of Class II MHC and CD86 when exposed to LPS or NP than cells
197 exposed to NPs or medium. The LPS used as a positive control for dendritic cell activation
198 resulted in CD86 and Class II MHC expression similar to that in NP-exposed dendritic cells.
199 These findings indicate that the cells recognized and were activated by PAH/TPP NPs.

200 A similar analysis of internalization was conducted using a human intestinal epithelial cells
201 line (HT-29). EPCAM was employed as a marker for epithelial cells, and various z-series

202 were acquired by confocal microscopy. Neither intracellular fluorescence nor hIL-8 secretion
203 was observed when epithelial cells were incubated with NPs. Pre-activated cells with TNF-
204 α (20 ng/mL) rendered no NP uptake (Figure S2A) nor production of hIL-8 (Figure S2B). As
205 a first approach to investigate the NP-driven secretion of mIL-1β in a phagocytic cell line,
206 we performed an LPS (1 μg/mL) prime stimulus followed by a dose-response of NPs. We
207 found that 0.5 mM NP (expressed as PAH monomer concentration) promoted the highest
208 level of secreted mIL-1β (Figure S2C).

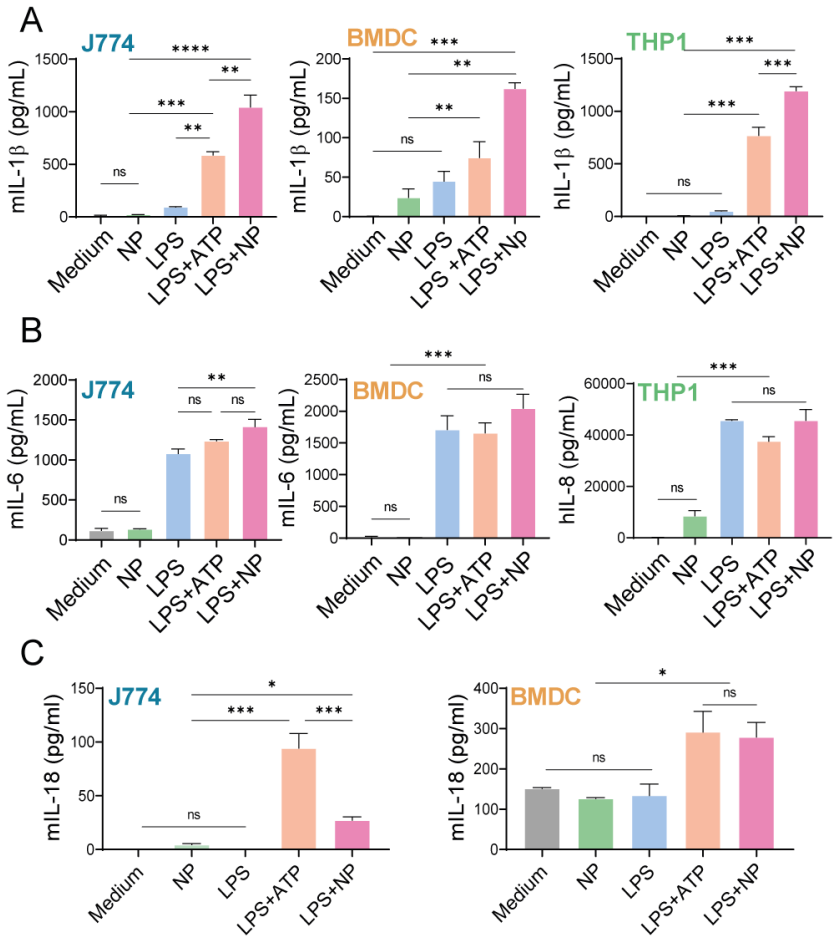

209

210 **Figure 4**. **Secretion of pro-inflammatory cytokine by macrophages, dendritic cells and monocytes.** J774,
211 THP-1 and BMDC were prime with LPS (1μg/mL) for 3h; the medium was fully replaced and stimulated with

212 ATP (50nM) for 3h as a positive control or with NP (0.5mM) overnight. Controls of LPS and NP were
213 stimulated overnight. **(A)** IL-1β and **(B)** IL-6 and IL-8 and **(C)** IL-18 secreted cytokine by phagocyte cells were
214 measured in supernatants by ELISA. All experiments were carried out in triplicate and data are expressed as
215 mean±SEM. P-value was determined by ordinary One-way ANOVA *P<0,05; **P<0,01; ***P<0,001;
216 ****p<0,0001.

217 We next investigated the production of pro-inflammatory cytokines by phagocytic cells
218 exposed to 0.5 mM NP or controls (Figure 4). We found a significantly higher level of IL-1β
219 in murine J774 macrophages and BMDCs, and human THP-1 monocytes exposed to
220 LPS+NP than cells exposed to LPS or NP (Figure 4A). We identified that the different cells
221 exposed to NPs did not significantly increase IL-1β concentration compared with the
222 medium; LPS+ATP was used as a positive control for IL-1β secretion.[51] These findings
223 collectively suggest that NP promoted IL-1β secretion and that LPS was necessary.
224 Nevertheless, the quantification of secreted mIL-6 and hIL-8 showed no significant changes
225 when cells were incubated with LPS or LPS+NP, indicating that the cytokine secretion was
226 independent of the NP presence (Figure 4B). Similarly, the cytokine levels were basal when
227 the cells were exposed to NP (Figure 4B). Furthermore, when we analyzed mIL-18, we
228 observed a differential secretion in J774 macrophages and BMDC incubated with LPS+NP.
229 Cells exposed to medium, LPS or NPs showed basal levels, whereas LPS+ATP or LPS+NP
230 induced the highest concentration of mIL-18 in BMDC (Figure 4C). These findings indicate
231 that the secretion of IL-1β and IL-18 in APCs required LPS and NP.

232

233 *Nanoparticles activate the intracellular inflammasome pathway*

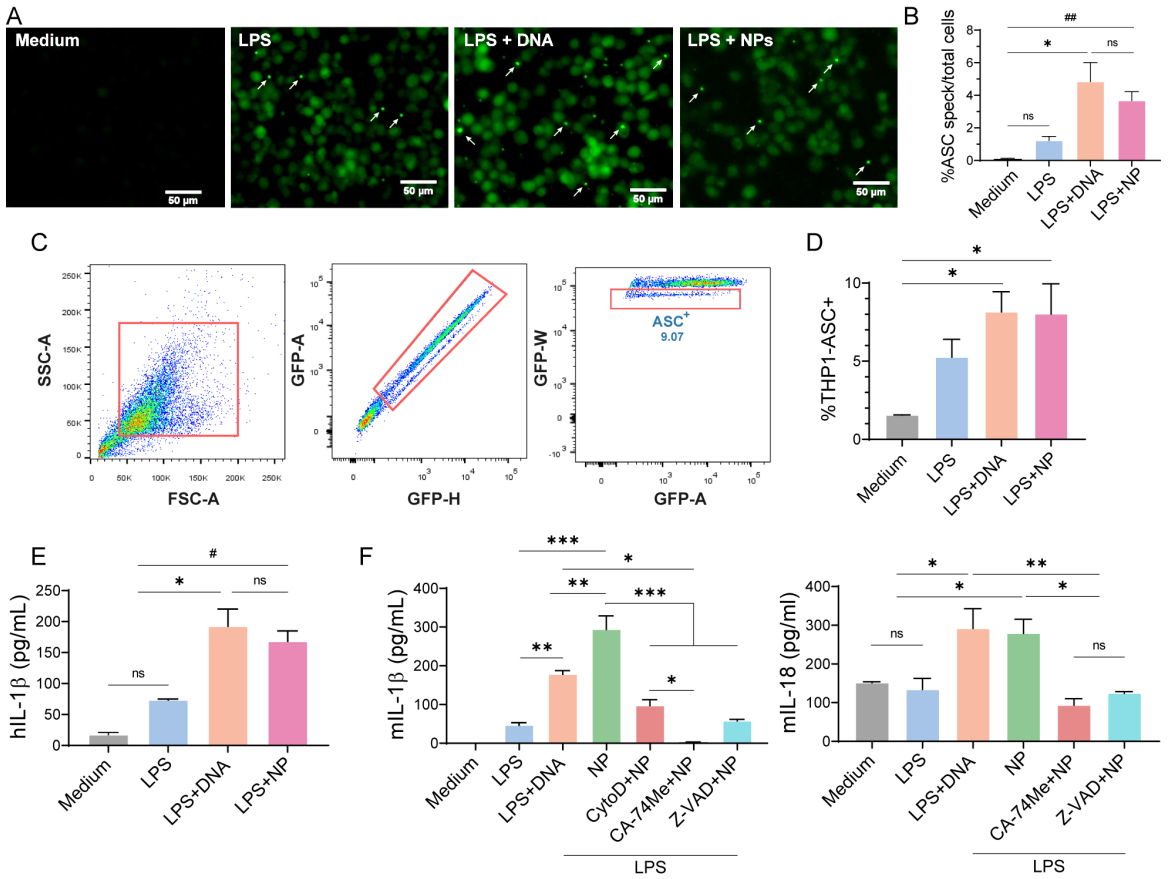

234

235 **Figure 5**. **Inflammasome activation and cytokine secretion in THP1-ACS-GFP cells and BMDC.** Cells
236 were primed with LPS for 3 hours. The medium was fully replaced, and the cells were either stimulated with
237 NP overnight or transfected with pcDNA as positive controls. **(A)** ASC-GFP specks within the cells are shown
238 with a white arrow, performed by epifluorescence microscopy; **(B)** Frequency of speck ASC-GFP^{+}cells. Three
239 independent experiments were performed. Each bar represents the average number of total speck^{+} cells/total
240 cells per field; 3 fields for each treatment were counted (2 replicates/treatment); **(C)** Flow cytometry gate
241 strategy to define ASC-GFP^{+}cells; **(D)** Frequency of speck ASC-GFP^{+}cells by flow cytometry; **(E)**
242 Quantification of secreted hIL-1β by ELISA. **(F)** BMDCs were pre-incubated with cytochalasin D (to inhibit
243 phagocytosis), CA-74Me (to inhibit cathepsin B), and Z-VAD-FMK (Z-VAD; to inhibit caspases) for 30
244 minutes prior to overnight stimulation with LPS+NP. The levels of secreted mIL-1β and mIL-18 were quantified
245 by ELISA.

246 All experiments were carried out in triplicate and data are expressed as mean±SEM. P-value was determined
247 by ordinary one-way ANOVA *p<0,05; **p<0,01; ***p<0,001 or t-Student #p<0,05; ##p<0,01.

248 Inflammasomes, such as NLRP3, require the adaptor molecule ASC to activate caspase-1.[52]
249 Following inflammasome activation, ASC assembles into a large protein complex, which can
250 be visualized as a "speck".[53] Representative pictures are shown with white arrowheads
251 indicating GFP-specks (Figure 5A). The number of specks in LPS+NP-treated cells was
252 significantly higher than in cells exposed to medium or LPS and equal to the positive control
253 with LPS+DNA ($p \leq 0.05$) (Figure 5B). This finding suggests that NP triggered the assembly
254 of the ASC complex. A similar analysis was performed using flow cytometry to quantify
255 ASC^+ cells,[54] and it was observed that cells exposed to LPS+DNA or LPS+NP had a
256 significantly higher frequency of ASC^+ cells compared to resting cells (Figure 5C and D).
257 The ratio of GFP-ASC^+ cells:total cells triggered by NPs was similar to the positive control
258 condition of LPS+DNA. Additionally, the quantification of hIL-1β in the supernatants
259 showed that LPS+DNA or LPS+NP induced higher levels of this cytokine than medium or
260 LPS ($p<0.05$) (Figure 5E). To investigate the inflammasome activation, we used different
261 pathway inhibitors. We found that cytochalasin D, the cathepsin B inhibitor CA-074Me and
262 the caspase inhibitor Z-VAD-FMK significantly suppressed the mIL-1β secretion induced
263 by LPS+NP ($p<0.001$) (Figure 5F). The analysis of the mIL-18 secretion showed similar
264 results, with a higher secretion in cells exposed to LPS+NP than in cells incubated with LPS
265 or medium, and the inhibitors suppressed the cytokine secretion (Figure 5F). Our results
266 suggest that NP promoted inflammasome activation through cathepsin B and caspase-1.
267 These findings led us to perform an experiment using inflammasome-null mice for NLRP3,
268 caspase-1/11, caspase-11 and gasdermin D (GSDMD). BMDM obtained from $NLRP3^{-/-}$,
269 $caspase1/11^{-/-}$, $caspase11^{-/-}$ and $GSDMD^{-/-}$ mice were incubated with 1μg/mL LPS and

270 0.5mM NP. To analyze the inflammasome activation, we quantified secreted mIL-1β and
271 mTNF-α by ELISA in the supernatants. We observed no mIL-1β secretion in cells stimulated
272 with LPS or NP in wild-type and KO mice. However, exposure to LPS+NP induced the
273 production and release of this cytokine in wild-type, caspase11$^{-/-}$ and GSDMD$^{-/-}$ BMDM. In
274 contrast, cells from NLRP3$^{-/-}$ and caspase1/11$^{-/-}$ mice showed decreased mIL-1β secretion
275 compared to wild-type animals ($p<0.001$) (Figure 6A). When the BMDM WT and caspase11^{-}
276 $^{/-}$ were stimulated with the positive control LPS+Nigericin, we detected the production of IL-
277 1β. Furthermore, the secretion of IL-1β in BMDM from NLRP3$^{-/-}$, caspase1$^{-/-}$ and GSDMD^{-}
278 $^{/-}$ was significantly abrogated (Figure 6A). The quantification of soluble mTNF-α showed
279 that cells from wild-type and KO mice secreted similar high amounts upon exposure to LPS,
280 LPS+NP or LPS+Nigericin. No TNF-α production was detected when cells were incubated
281 with NP (Figure 6B). LDH measured in the supernatants showed that the stimuli did not
282 significantly affect the cells. The consistent level of soluble LDH in cells exposed to the
283 medium, NP or LPS+NP indicated that cell viability was unaffected (Figure S3A).
284 Additionally, the lysate of LPS+NP-exposed cells from wild-type or KO mice showed a
285 minimal difference in the activation of caspase-1 (20 kDa) between cells derived from wild-
286 type and NLRP3$^{-/-}$ mice. Inactive caspase-1 was detected in resting and LPS+NP-stimulated
287 cells, while it was absent in samples from cells of caspase1/11$^{-/-}$ animals (Figure S3B).

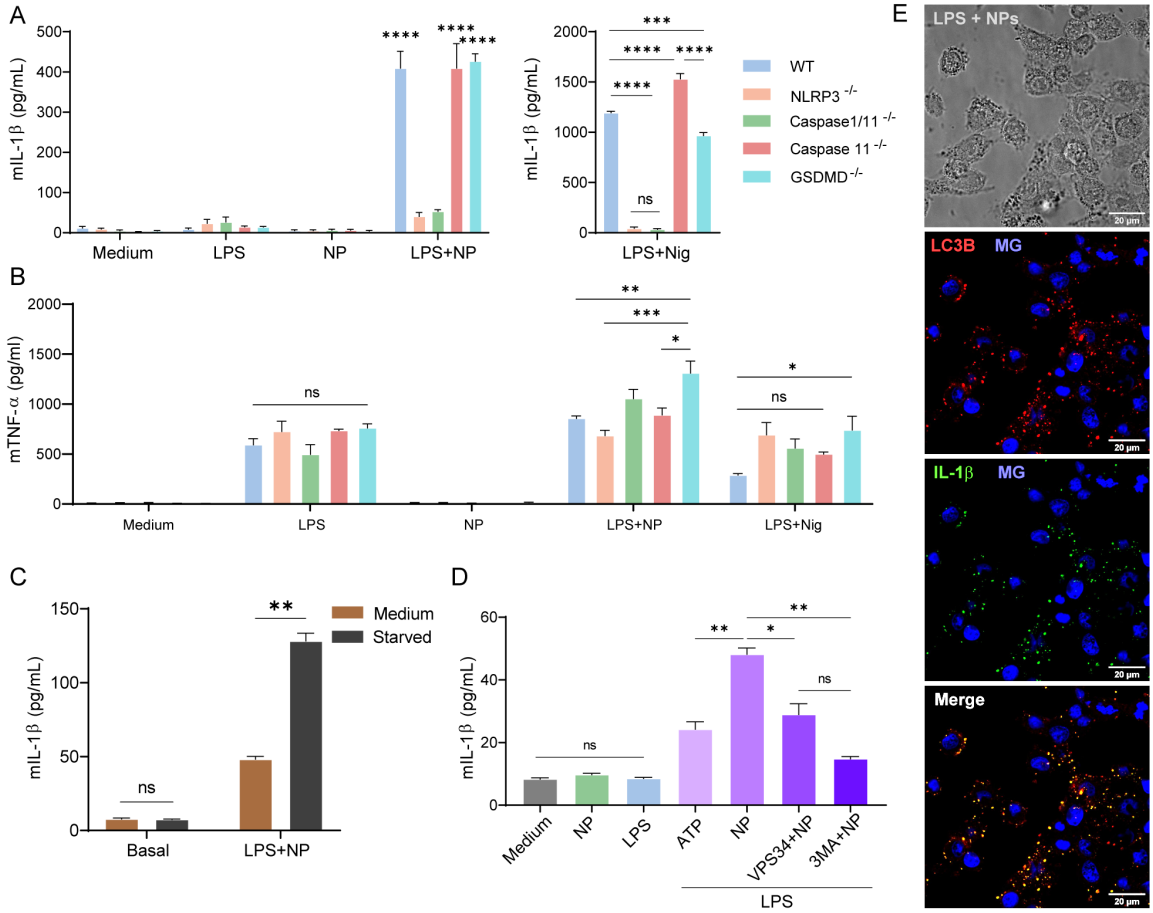

Figure 6. Inflammasome pathway analysis in BMDM from C57BL/6 (WT), NLRP3$^{-/-}$, Casp1/11$^{-/-}$, Casp11$^{-/-}$, GSDMD$^{-/-}$ mice. Cells were stimulated with LPS, NP, or LPS+NP, and **(A)** mIL-1β, **(B)** mTNFα were measured in supernatants by ELISA. The effect of autophagy stimulation by starvation on macrophage IL-1β secretion was investigated in J774 cell lines. After being primed for 3 hours with LPS, the cells were treated with NP. Six hours later, the cells were either left untreated in medium or had their supernatants replaced with Earle's Balanced Salt Solution (EBSS) for an additional hour of culture and quantification **(C)** mIL-1β in the supernatants by ELISA. J774 cell line were stimulated for 6h with NP in the presence of inhibitors of the autophagy VPS34-IN1 and 3-methiladenine (3-MA) and quantification **(D)** mIL-1β. **(E)** Cytokine mIL-1β colocalized with LC3B by confocal microscopy after 6 hours of stimulation with LPS+NP (MG: Methyl green). Data are expressed as mean±SEM. P-value was determined by ordinary one-way ANOVA *P<0,05; **P<0,01; ***P<0,001; ****p<0,0001.

300 As mentioned before, we found that the release of mIL-1β was independent of GSDMD
301 (Figure 6A). This prompted us to study the secretion of IL-1β. Among the multiple pathways
302 described in myeloid cells, we investigated autophagy as responsible for the secretion of IL-
303 1β. As starvation has been reported to induce autophagy,[55,56] we performed experiments
304 using the EBSS starvation medium following cell activation. We observed a significant
305 increase in the production of mIL-1β when macrophages were stimulated with LPS+NP and
306 then subjected to starvation with EBSS medium compared to the cells that were stimulated
307 with LPS+NP (Figure 6C). To confirm this finding, we used 3-methyladenine (3-MA)
308 (blocker of early stages of autophagy) and VPS34-IN1 (inhibitor of the class III PI3K) as
309 autophagy inhibitors. All treatments significantly decreased the mIL-1β secretion in cells
310 exposed to LPS+NP (Figure 6D). To confirm if autophagy is involved in the secretion of
311 mIL-1β, we measured a pro-inflammatory cytokine (mIL-6) that is released through the
312 canonical ER-Golgi and independent of the autophagy pathway. We observed unchanged
313 high levels of mIL-6 in cells exposed to LPS+NP irrespective of the presence of EBSS
314 (Figure S3C). However, when the different inhibitory conditions were assessed, we found
315 that 3-MA led to a not significantly decreased cytokine level (Figure S3D). Nevertheless, it
316 is essential to note that this effect was negligible compared to that exerted on mIL-1β
317 secretion (Figure 6D). Additionally, we did not observe a significant increase in the release
318 of LDH in the cells, either with or without the autophagy inhibitors (Figure S3E). Moreover,
319 we observed similar results regarding IL-1β secretion when BMDC were treated with the
320 autophagy inhibitors (Figure S3F). Finally, we found by confocal microscopy that mIL-1β
321 co-localized with LC3B, a central protein in the autophagy pathway and autophagosome
322 biogenesis, when macrophages were stimulated with LPS+NP (Figure 6E) compared to cells
323 incubated with medium, NP or LPS (Figure S3G).

324 Overall, these findings confirmed that the NLRP3-dependent inflammasome pathway was
325 involved in cell activation with IL-1β production, and that autophagy was involved in the
326 secretion of IL-1β induced by LPS+NP. However, considering the reduced level of mIL-1β
327 in cells from NLRP3$^{-/-}$ mice compared with wild-type animals and the active caspase-1
328 observed in lysates of NLRP3$^{-/-}$ cells (Figure S3B), we suggest that an NLRP3-independent
329 inflammasome pathway may also be involved in mIL-1β production. Besides, the consistent
330 level of soluble LDH in cells exposed to the medium, NP or LPS+NP indicated that cell
331 viability was unaffected upon activation.

332

333 *The systemic administration of NP-OVA triggered a specific humoral and cellular immune*
334 *response in mice*

335 To characterize its adjuvanticity *in vivo*, we first measured the presence of LPS in PAH, TPP
336 and NP with the human TLR4 HEK reporter cells, which secreted SEAP as readout. We
337 found that the SEAP activity was comparable to that in non-stimulated cells and lower than
338 0.01 ng/mL of LPS (Figure S4). Next, we analyzed the ability of NPs to encapsulate proteins.
339 Considering previous results where we demonstrated that PAH/TPP nanoparticles can
340 encapsulate a wide range of proteins such as lysozyme, cytochrome C oxidase, bovine serum
341 albumin, and glucose oxidase,[44] we tested the encapsulation of ovalbumin (OVA) as a model
342 protein. The protein loading was carried out during the ionic crosslinking step in the synthesis
343 of the NPs. Specifically, the protein was incorporated prior to the addition of TPP, forming
344 PAH/OVA adducts that were then ionically crosslinked by the action of the TPP anion
345 (Figure S5A). Although the protein encapsulation mechanism is not yet fully elucidated, we
346 believe that proteins act as ionic crosslinkers to form three-component coacervates. In the

347 case of OVA, whose isoelectric point is below physiological pH, it exposes negative surface
348 charges, making it suitable as an ionic crosslinker for positively charged PAH. The analysis
349 of OVA content in the supernatant after centrifuging the colloidal dispersion of
350 PAH/OVA/TPP NPs (NP-OVA) showed that the encapsulation percentage is dependent on
351 the OVA concentration used, with approximately 35% of protein encapsulated for 100 μg/mL
352 OVA (Figure S5B).

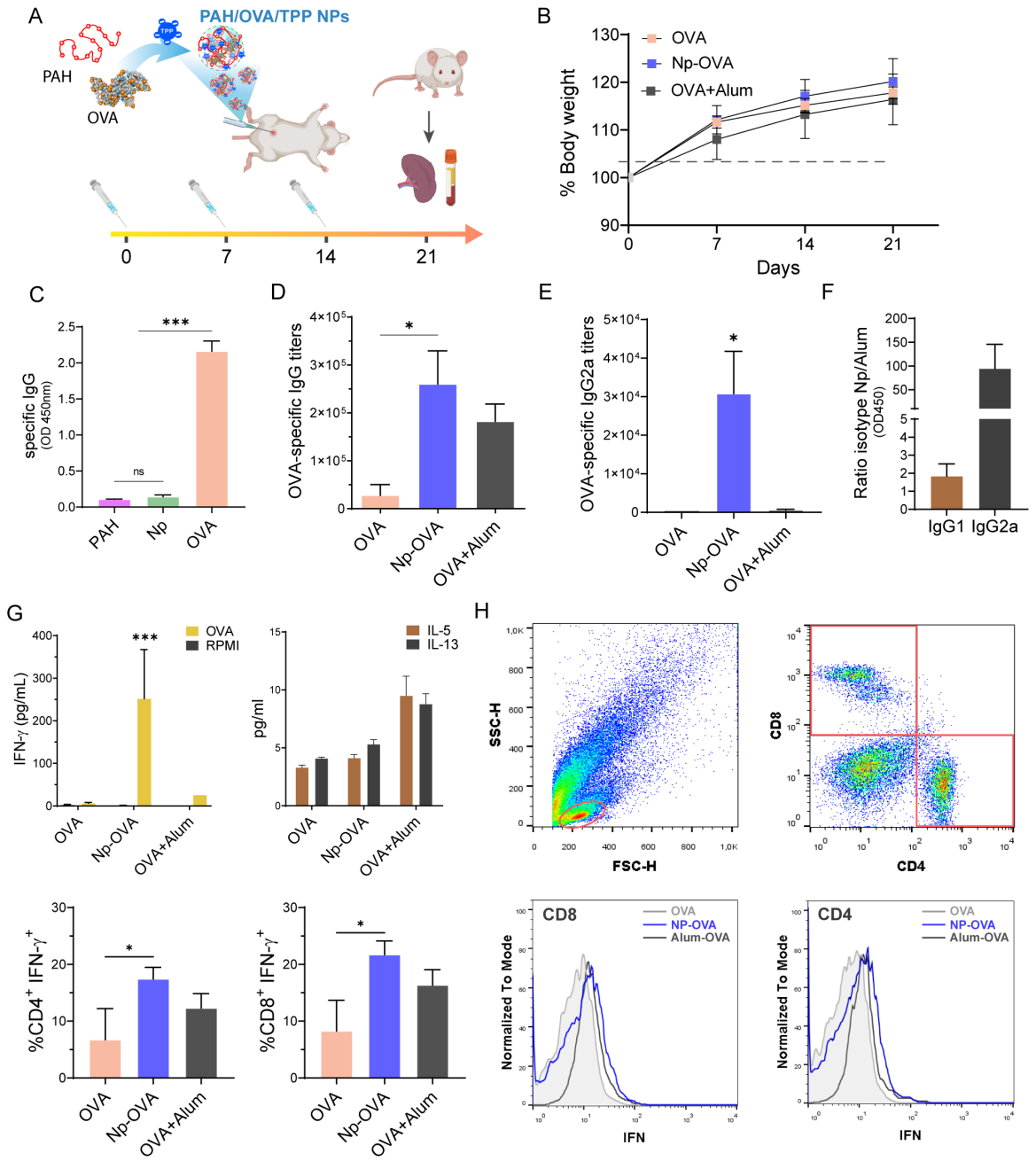

353

354 **Figure 7. Intraperitoneally immunization of Balb/c mice with NP-OVA and specific humoral and cellular**
355 **immune responses. (A)** Immunization scheme; **(B)** Body weight monitoring; **(C)** quantification of serum
356 specific IgG to PAH, NP and OVA and **(D)** OVA-Specific IgG and **(E)** IgG2a titers in serum of immunization
357 animals and **(F)** serum optical density ratio of isotypes (IgG1 and IgG2a) between NP-OVA and OVA+Alum;
358 **(G)** Quantification of mIFN-γ, mIL-5 and mIL-13 in the supernatants of spleen cells from immunized mice

359 assessed by ELISA (top panel). Quantification for $CD4^+IFN\text{-}\gamma^+$ and $CD8^+IFN\text{-}\gamma^+$ T cells (lower panel). **(H)**
360 Spleen cells from immunized mice were incubated with brefeldin A for the last 4h of culture and then were
361 stained with anti-CD4 (PerCP-Cy5.5) or anti-CD8 (APC); flow cytometry gate strategy and Mean Fluorescent
362 Intensity (MFI). The immunization experiment was carried out in duplicate, and all experiments were performed
363 in triplicate; data are expressed as mean±SEM. P-value was determined by ordinary one-way ANOVA *p<0,05;
364 **p<0,01; ***p<0,001 or t-Student test #p<0,05.

365

366 To analyze the immune response, mice were intraperitoneally injected with NP-OVA in 3
367 weekly doses (Figure. 7A). As a control, we administered a formulation containing the
368 approved adjuvant for human use, aluminum hydroxide (Alum),[57] with OVA. No weight loss
369 was observed during the whole experiment (Figure 7B). We did not observe specific
370 antibodies to the nanoparticle or the polymer PAH in animals immunized with NP-OVA
371 (Figure 7C). Animals that received NP-OVA produced higher levels of serum OVA-specific
372 IgG than mice injected with OVA ($p<0.01$) and similar values compared with mice that
373 received OVA+Alum (Figure. 7D). The subclass analysis revealed that NP-OVA induced
374 higher titers of OVA-specific IgG2a than in mice injected with OVA+Alum (Figure 7E); in
375 addition, the ratio of IgG subclasses in NP-OVA and OVA+Alum injected mice showed a
376 higher production of OVA-specific IgG2a in NP-OVA immunized animals (Figure 7F). To
377 analyze the T cell-mediated immune response, spleen cells from mice immunized with NP-
378 OVA, OVA+Alum and OVA were stimulated with OVA and cytokines were measured in
379 the supernatants. We found that mice immunized with NP-OVA induced increased levels of
380 IFN-γ when cells were stimulated with OVA ($p<0.001$). Cells from mice that received OVA
381 or OVA+Alum did not secrete IFN-γ (Figure 7G). On the other hand, the Th2 cytokines mIL-
382 5 and mIL-13 showed decreased concentration in NP-OVA-treated mice compared to those

383 administered with OVA+Alum (Figure 7G). To further evaluate the cell source of IFN-γ,
384 spleen cells were analyzed by intracellular cytokine staining following *in vitro* OVA
385 stimulation. We found that the frequency of $CD4^{+}IFN\text{-}\gamma^{+}$ and $CD8^{+}IFN\text{-}\gamma^{+}$ lymphocytes was
386 significantly increased in mice immunized with NP-OVA (Figure 7H). Overall, these
387 findings support that NP-OVA promoted the induction of a Th1-dependent immune response
388 with specific IgG and IgG2a, and $CD4^{+}IFN\text{-}\gamma^{+}$ and $CD8^{+}IFN\text{-}\gamma^{+}$ T cells following the
389 immunization with OVA adjuvanted with NP.

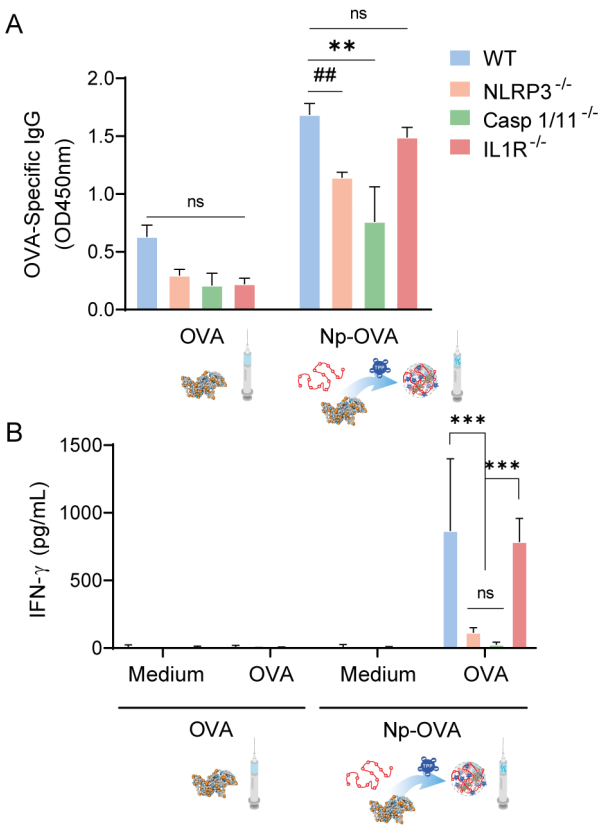

390

391 **Figure 8. Intraperitoneal immunization with NP-OVA in WT and KO C57BL/6 mice and specific**
392 **humoral and cellular response**. C57BL/6 (WT), $NLRP3^{-/-}$, $Casp1/11^{-/-}$, $IL\text{-}1R^{-/-}$ mice were immunized
393 following the same scheme as in Figure 6A. **(A)** Measurement of serum OVA-specific IgG in serum (dilution
394 1/100) by ELISA and **(B)** secreted mIFN-γ by spleen cells from OVA or NP-OVA immunized mice by ELISA.
395 The immunization experiment was carried out in duplicate and all experiments were performed in triplicate;

396 data are expressed as mean±SEM. P-value was determined by ordinary one-way ANOVA *p<0,05; **p<0,01;
397 ***p<0,001 or t-Student test ##p<0,01.

398 To investigate the role of the inflammasome pathway in promoting the specific immune
399 response, C57BL/6 mice wild-type and NLRP3$^{-/-}$, caspase1/11$^{-/-}$ and IL-1R$^{-/-}$ mice were
400 intraperitoneally immunized with NP-OVA. As shown in Figure 8A, NLRP3$^{-/-}$ and
401 caspase1/11$^{-/-}$ mice exhibited lower levels of serum OVA-specific IgG than wild-type mice
402 ($p<0.01$), whereas IL1-R null mice showed similar levels than wild-type mice (Figure 8A).
403 Finally, spleen cells from wild-type and KO mice were stimulated with OVA or medium,
404 and IFN-γ levels were measured in the supernatants. We found that cells from wild-type mice
405 immunized NP-OVA showed higher levels of IFN-γ than cells from WT mice that received
406 OVA, as well as NLRP3$^{-/-}$ and caspase1/11$^{-/-}$ mice administered with NP-OVA. Additionally,
407 cells from IL1-R$^{-/-}$ mice injected with NP-OVA showed a similar concentration of IFN-γ to
408 WT animals (Figure 8B). These findings indicate that the NLRP3 pathway is critical in
409 promoting the OVA-specific Th1-dependent immune response.

410

411 **DISCUSSION**

412 Our findings showed that NPs are exclusively internalized by phagocytic antigen-presenting
413 cells, specifically dendritic cells and macrophages. Subsequently, they localize intracellularly
414 within the endosome compartment, causing their disruption and leading to the translocation
415 of their components into the cytosol. Thus, the internalization of NP triggers the cellular
416 activation and inflammasome assembly, releasing the pro-inflammatory cytokines IL-1β and
417 IL-18 to the extracellular medium. Remarkably, we did not observe the NP internalization in
418 non-phagocytic mucosa epithelial cells. The permeabilization of the lysosomal membrane is
419 one of the most frequently described mechanisms for activating the inflammasome by
420 particles and NP.[58,59] We used several inhibitors to confirm the role of the different
421 components of the pathway, and we corroborated the participation of cathepsin B as the early
422 activator of the inflammasome.[60,61] Then, using BMDM KO mice, we confirmed that cell
423 activation followed by IL-1β secretion is NLRP3- and caspase-1- dependent and caspase-11-
424 and gasdermin-D-independent with no induction of cellular death by pyroptosis.[62] The
425 literature shows that the non-canonical autophagy pathway is involved in the secretion of
426 inflammatory molecules such as IL-1β and HMGB1.[63,64] In macrophages and monocytes,
427 LC3B is essential for the efficient secretion of IL-1β in response to lysosomal damage.[56,65]
428 In this sense, we demonstrated that the inflammasome activation proceeded with autophagy
429 induction for secreting IL-1β. All together, these findings demonstrated that PAH-based NP
430 activated phagocytic cells with increased expression of MHC II and CD86, along with the
431 secretion of IL-1β and IL-18, without inducing cell death, which make them a candidate
432 adjuvant to trigger an antigen-specific immune response.

433 It is known that aluminum salts, such as the extensively used in human vaccines aluminum
434 hydroxide (alum), can enhance the effectiveness of the immune response by activating
435 antigen-presenting cells through the depot effect and the aggregation of antigens to improve
436 the uptake and activation of APCs. Furthermore, it has been described that alum triggered
437 the NLRP3-dependent inflammasome pathway to further promote adaptive immunity and
438 memory.[66] Thus, we evaluated the *in vivo* adjuvant capacity of PAH/TPP NP in mice that
439 were systemically administered with OVA encapsulated in NP. We observed the induction
440 of innate immunity via the inflammasome-dependent pathway to further promote a Th1-
441 driven adaptive humoral and cellular immunity. Our findings showed the induction of serum
442 IgG and IgG2a-specific antibodies and the expansion of $CD4^+$- and $CD8^+$-IFN-γ-producing
443 T cells. Furthermore, we confirmed *in vivo* that the Th1-dependent isotype synthesis and
444 IFN-γ production were NLRP3- and caspase-1-dependent. It is reported that the NLRP3
445 inflammasome pathway initiates a caspase-1–dependent IL-1β and IL-18 secretion
446 promoting interferon-γ production and Th1 differentiation.[67,68] Similar to other adjuvants,
447 such as Alum and QS-21, PAH-based nanoparticles, along with LPS as a first inflammasome
448 activation signal, induced *in vitro* the NLRP3-ASC-caspase-dependent IL-1β production. *In*
449 *vivo*, however, the first signal may be triggered by a DAMP, such as uric acid, generated at
450 the immunization site.[69,70] Additionally, IL-18, constitutively expressed by several cell types,
451 can stimulate IL-1β transcription and may initiate a pro-inflammatory cascade during
452 vaccination.[71] The *in vivo* induction of OVA-specific $CD8^+$T cells indicates that NP-OVA
453 triggered the cross-presentation of OVA, which may proceed upon the endosome is disrupted
454 and the content is translocated into the cytosol. Further studies are needed to confirm if
455 macrophages and dendritic cells contribute to this mechanism, which is critical when
456 considering using PAH-based NP as an adjuvant in an anti-tumoral or viral vaccine.

457 Muñoz-Wolf et al. reported that polymeric nanoparticles made of poly-lactic-co-glycolic acid
458 with a diameter of 50-60nm elicited a robust cellular immune response through the caspase-
459 11- and the pyroptosis effector gasdermin D-dependent non-canonical inflammasome
460 pathway. They described a division of labor for IL-1β and IL-18 to induce the appropriate
461 immunogenic context for Th1 and $CD8^+$ T cell induction, respectively.[72] In our study, we
462 characterized a polymeric nanoparticle of PAH that activated murine and human
463 macrophages and dendritic cells through the canonical caspase-1- and NLRP3-dependent
464 inflammasome pathway with the secretion of IL-1β and IL-18, without cell death, and
465 independent of caspase-11 and gasdermin D-dependent pyroptosis[73,74]. We found that PAH-
466 based NP induced autophagy for the secretion of the pro-inflammatory cytokine IL-1β.

467 **CONCLUSION**

468 In summary, we characterized a novel polyallylamine-based self-assembled nanoparticle as
469 a systemic and safe adjuvant, demonstrating its ability to target the encapsulated OVA
470 immunogen to phagocytic cells efficiently. This targeting enabled antigen-presenting cells to
471 acquire the capacity to activate T cells, thereby inducing a robust Th1-dependent humoral
472 and cellular immune response. The ability of this nanosystem to enhance the immune
473 system's recognition and response to the antigen highlights its potential for biomedicine.
474 These findings advance our understanding of nanoparticle-based adjuvants and pave the way
475 for designing and developing innovative nanoparticle-based systemic vaccines, which could
476 be used to treat a wide range of infectious and non-infectious diseases, potentially
477 transforming vaccine strategies in immunotherapy.

478 **MATERIALS AND METHODS**

479 **Preparation and characterization of PAH/TPP nanoparticles**

480 PAH/TPP nanoparticles were prepared by following the procedure described in Apuzzo et
481 al[45]. Briefly, 0.125 V_f ml of PAH (17.5 kDa, Sigma-Aldrich, St. Louis, MO, USA) 40mM
482 (monomer concentration) at pH 8.5, 0.75 V_f ml of deionized water, and 0.125 V_f ml of TPP
483 (Sigma-Aldrich, St. Louis, MO, USA) 24mM at pH 8.5 were mixed under constant stirring
484 at room temperature (RT). The addition of TPP was made very quickly to prevent the system
485 from collapsing into a macroscopic phase. After this procedure, a volume V_f of dispersed
486 PAH/TPP nanoparticles is obtained with a final concentration of PAH and TPP of 5mM and
487 3mM, respectively. In this work, the NP concentration was expressed in terms of PAH
488 monomer concentration (i.e., 0.5mM NP means a 1:10 dilution of the original dispersion).
489 The protein-loaded nanoparticle dispersions were prepared by following the same procedure
490 but adding an aqueous solution of chicken egg albumin (OVA) (EndoFit(TM) InvivoGen, San
491 Diego, CA, USA) at the water addition stage. The volume of deionized water was re-
492 calculated as $V_{water} = 0.75\ V_f - V_{OVA}$ and the OVA volume was fixed to obtain the desired
493 OVA concentration in the final solution. The percentage of encapsulated OVA was calculated
494 by assessing the protein content of the supernatant using bicinchoninic acid (BCA)
495 commercial kit (Thermo Fisher Scientific, Waltham, MA, USA).

496 Atomic force microscopy (AFM) images were taken with an Agilent 5500 SPM in tapping
497 mode at room temperature using PPP-NCL (NANOSENSORS™) silicon tips. For the sample
498 preparation, a droplet of the suspended PAH/TPP NPs was placed on top of a freshly cleaved
499 highly oriented pyrolytic graphite (HOPG) substrate, rested for 2 min, rinsed with Milli-Q
500 water, and dried with N_2. Transmission electron microscopy (TEM) images were acquired
501 with a JEOL microscope (120 kV) equipped with a Gatan US1000 CCD camera. For the

502 TEM sample preparation, 5 µl of a PAH/TPP NPs dispersion was placed in a carbon-coated
503 copper grid and stained with phosphotungstic acid to create image contrast. Dynamic light
504 scattering (DLS) and ζ-potential measurements were performed using a ZetaSizer Nano
505 (ZEN3600) at 20 °C using disposable cuvettes. Hydrodynamic diameter was measured using
506 a 173° backscatter angle with 20 runs per sample, averaging 5 measurements. ζ-potential was
507 calculated from electrophoretic mobility with 100 runs per sample. Confocal
508 (epifluorescence) microscopy of PAH/TPP NPs was carried out using a Carl Zeiss Axio
509 Observer 7 with a Plan-Apochromat 63x/1.40 Oil DIC M27 objective.
510
511 **Cell lines**
512 HEK-hTLR4-reporter (InvivoGen®, San Diego, CA, USA), HT-29 and J774 cell lines were
513 maintained in DMEM medium (Gibco® Thermo Fisher Scientific, Waltham, MA, USA)
514 containing 10% FBS (Internegocios, Mercedes, Bs As, Argentina), 100U/mL penicillin and
515 100µg/mL streptomycin (Gibco® Thermo Fisher Scientific, Waltham, MA, USA). The
516 THP1-ASC-GFP cell line was maintained in RPMI medium (Gibco® Thermo Fisher
517 Scientific, Waltham, MA, USA) containing 10% FBS, 100U/mL penicillin and 100µg/mL
518 streptomycin.

519 Bone marrow-derived macrophages (BMDMs) were cultured in DMEM medium, and bone
520 marrow-derived dendritic cells (BMDC) were cultured in RPMI medium containing 10%
521 FBS, 100U/mL penicillin and 100µg/mL streptomycin. Both cells were derived from wild-
522 type (WT) and knockout (KO) mice with 20% L929-conditioned medium (LCCM) in
523 DMEM and 20ng/mL recombinant granulocyte-macrophage colony-stimulating factor (GM-
524 CSF) (R&D Systems, Minneapolis, MN, USA) in RPMI for BMDM and BMDC,

525 respectively. Briefly, bone marrow cells were obtained from the femur and tibia of WT or
526 KO mice[75]. Cells were seeded on dish plate $5x10^5$ cell/mL (day 0) and maintained in a
527 conditioned medium and GM-CSF containing 10% FBS, 100U/mL penicillin and 100µg/mL
528 streptomycin at 37°C, in a 5% CO_2 atmosphere for 7 days. On day 4, the medium was fully
529 replaced, and cells were stimulated with 0.5mM PAH/TPP NPs. As a positive control for
530 inflammasome activation, cells were treated with 5mM Nigericin for 50min, after being
531 primed with 1µg/mL LPS from *E. coli* (LPS E. coli) (Sigma-Aldrich, St. Louis, MO, USA)
532 for 3h at 37°C. Supernatants were collected and cells were lysed with 25µL/well M-PERR
533 (Thermo Fisher Scientific, Waltham, MA, USA) supplemented with 1:100 protease inhibitor
534 cocktail (Sigma-Aldrich, St. Louis, MO, USA). Both supernatants and cell lysates were
535 stored at −80°C until used.

536

537 **Cell stimulation with NP and characterization**

538 *Flow cytometry for phenotype and cell activation characterization:* BMDC were seeded in
539 24-well microplates at $1x10^6$ cells/well and stimulated with ultrapure 1µg/mL LPS from *E.*
540 *coli* for 3h at 37°C, followed with 0.5mM PAH/TPP NPs overnight (ON). BMDC were
541 washed with PBS and stained for 1h at 4°C with anti-CD11c (PE), anti-CD11b (PerCP-
542 Cy5.5), anti-MHCII (APC) and anti-CD86 (FITC) (Thermo Fisher Scientific, Waltham, MA,
543 USA). As a positive control for inflammasome induction, cells were primed with ultrapure
544 1µg/mL LPS from *E. coli* for 3h, followed by 5mM ATP (Sigma-Aldrich, St. Louis, MO,
545 USA) for 3h at 37°C. For inhibition analysis, cells were pre-treated for 30min with 100µg/mL
546 Z-VAD-FMK (Sigma-Aldrich, St. Louis, MO, USA), 1µg/mL cytochalasin D (Santa Cruz
547 Biotechnology Inc, Santa Cruz, CA, USA) or 50µM CA-74ME (Santa Cruz Biotechnology

548 Inc, Santa Cruz, CA, USA) and kept in culture during the experiment. Fluorescence
549 acquisition was performed with a FACS Aria Fusion cytometer, and data was analyzed using
550 FlowJo software.

551 *Reagents for inhibitions:* For inhibition analysis, cells were pre-treated for 30min with
552 100µg/mL Z-VAD-FMK, 1µg/mL cytochalasin D or 50µM CA-74ME, 5mM 3-methyl
553 adenine (Cayman, Ann Arbor, MI, USA) and 1 µM VPS34-IN1 (Cayman, Ann Arbor, MI,
554 USA) and 100nM Bafilomycin A1 (Cayman, Ann Arbor, MI, USA) and kept in culture
555 during the experiment. When indicated, at 4 hours post-NP stimulation, supernatants were
556 removed and replaced with either complete medium or Earle's Balanced Salt Solution
557 (EBSS) for medium starvation.

558 *Nanoparticle internalization analysis:* BMDC and BMDM were grown on glass coverslips
559 and stimulated ON with 0.5mM FITC-PAH/TPP NP. Poly (fluorescein isothiocyanate
560 allylamine hydrochloride), Mw~56000 (Sigma-Aldrich, St. Louis, MO, USA) was used
561 instead of PAH in the PAH/TPP formulation. Cells were fixed for 30min in 4%
562 paraformaldehyde (PFA) at RT and nuclei were stained with 1µg/mL propidium iodide (IP)
563 (Sigma-Aldrich, St. Louis, MO, USA). Cells were washed with PBS, blocked with 2% BSA
564 in phosphate buffer pH=7.4 for 30min at RT and incubated with mouse anti-human LAMP1
565 (BD Biosciences, Franklin Lakes, NJ, USA) for 1h at RT, followed with anti-mouse Alexa
566 647 (Abcam, Cambridge, UK) for 1h at RT. Cells were washed, coverslips were mounted
567 onto a slide containing 10µL of fluorescence mounting media (Dako, Abcam, Cambridge,
568 UK) and allowed to dry at 4°C ON. Fluorescence was analyzed with a Leica SP5 Confocal
569 Microscope.

570 *Internalization inhibition assay:* BMDC and J774 were stimulated with 0.5mM FITC-
571 PAH/TPP NPs and phagocytosis was inhibited with 1µg/mL cytochalasin D. Cells were
572 characterized by flow cytometry with anti-CD11b (Percp-Cy5.5) and anti-F4/80 (APC)
573 (Thermo Fisher Scientific, Waltham, MA, USA) and confocal microscopy for intracellular
574 fluorescence. Nuclei were stained with 1µg/mL IP.

575 *Intracellular immunostainings for the localization of IL-1β in autophagosomes: The* J774
576 cell line was grown on glass coverslips and prime for 3h at 37°C with 1µg/mL LPS from E.
577 coli, followed with 0.5mM PAH/TPP NP for 6h. After fixation with PFA 4% for 30 min,
578 cells were blocked with PBS-glycine (0.1 M) for 15 min, permeabilized with acetone (−20°C)
579 for 7min, and blocked with PBS-BSA 5% for 1h at RT. Then, macrophages were incubated
580 with the rabbit polyclonal anti-LC3B (Proteintech, Rosemont, IL, USA) and mouse
581 polyclonal anti-IL-1β (Cell Signaling Technology, Danvers, MA, USA) in blocking buffer
582 ON at 4°C and then incubated with the secondary anti-rabbit Alexa 594 (Abcam, Cambridge,
583 UK) and anti-mouse Alexa 488 (Invitrogen, Thermo Fisher Scientific, Waltham, MA, USA)
584 antibodies for 1h at RT. Nuclei were stained with methyl green (Sigma-Aldrich, St. Louis,
585 MO, USA) and mounted onto a slide containing fluorescence mounting media (Dako,
586 Abcam, cambrige, UK). Image acquisition was performed with an SP5 Leica Confocal
587 Microscope.

588 *Epithelial cell stimulation:* HT-29 cells were maintained in DMEM containing 10% FBS,
589 100U/mL penicillin and 100µg/mL streptomycin at 37°C with 5% CO_2, and $3x10^4$ cells/well
590 were seeded in 96-well microplates. Cells were incubated ON to 70% confluence and the
591 medium was fully replaced. Then, cells were stimulated ON with 0.5mM FITC-PAH/TPP
592 NP, or with 50ng/mL TNF-α (R&D Systems, Minneapolis, USA) for 30min at 37°C followed

593 with FITC-PAH/TPP NP. A mouse monoclonal anti-human EPCAM (Santa Cruz
594 Biotechnology, Santa Cruz, CA, USA) antibody, followed bywith an anti-mouse Alexa 647
595 conjugated antibody (Abcam, Cambridge, UK), was used for epithelial cell detection. Cell
596 fluorescence was analyzed with an SP5 Leica Confocal Microscope.

597 *Inflammasome activation assessment*: THP1-ASC-GFP were maintained in RPMI medium
598 containing 10% FBS, 100U/mL penicillin and 100µg/mL streptomycin at 37°C in a 5% CO_2
599 atmosphere and plated at 3.6×10^5 cells/well in 96-well plates. Cells were stimulated with
600 0.5mM PAH/TPP NP or primed with ultrapure 1µg/mL LPS from *E. coli* followed with
601 0.5mM PAH/TPP NP ON. For a positive control, cells were primed with 1µg/mL LPS from
602 *E. coli* for 3h and transfected with 500ng/mL bacterial plasmid cDNA. pcDNA was generated
603 by cloning the PCR-generated full-length cDNA from a random non-related gene.
604 Transfection was carried out with Lipofectamine™ LTX Reagent with PLUS TM Reagent
605 (Invitrogen, Thermo Fisher Scientific, Waltham, MA, USA), following the manufacturer´s
606 instructions. Supernatants were harvested and stored at −80°C until used and cells were
607 stained with DAPI (nuclear staining) (Invitrogen, Thermo Fisher Scientific, Waltham, MA,
608 USA) and fixed with 2% PFA fixation for the microscopy analysis.
609 The frequency of ASC-GFP$^+$ cells and localization of fluorescent ASC specks were assessed
610 using a Nikon Eclipse Ti Fluorescence Microscope and analyzed with ImageJ software. The
611 total cells: ASC-GFP$^+$ cells ratio was calculated.

612 *Quantification of secreted cytokines:* Supernatants of stimulated BMDM, J774, BMDC,
613 THP1, THP1-ASC-GFP and HT-29 cells were assessed for mIL-1β, mIL-18, mIL-6, mIFN-
614 γ and mTNF-α using the Mouse DuoSet R&D Systems ELISA kit. The concentration of hIL-
615 1β and hIL-8 were measured using a human Invitrogen ELISA Kit (Thermo Fisher Scientific,

616 Waltham, MA, USA). All the protocols were used according to the manufacturer's
617 instructions. The concentration of released LDH (enzymatic assay) (LDH-L Weiner Lab,
618 Rosario, Santa Fe, Argentina) was quantified.

619 *Immunoblotting analysis*: Cell lysates and supernatants were analyzed by SDS-PAGE
620 followed by immunoblotting. Proteins suspended in loading buffer (SDS+β-
621 mercaptoethanol) were separated on a 15% SDS-PAGE gel, and transferred onto
622 nitrocellulose membranes (Amersham Biosciences, Uppsala, Sweden) using transfer buffer
623 (50mM Tris, 40mM glycine, 10% methanol). After blocking for 1h in TBS with 0.1% Tween-
624 20 containing 5% non-fat dry milk, membranes were incubated overnight at 4°C with a
625 mouse monoclonal antibody to the p20 subunit of caspase-1 (Adipogen, San Diego, CA,
626 USA) at a 1:1,000 dilution. A loading control blot was performed with an anti–β-actin
627 monoclonal antibody (Cell Signaling Technology, Danvers, MA, USA) at a 1:1,000 dilution.
628 Following three washes in TBS with 0.1% Tween 20, membranes were incubated for 1h at
629 RT with the appropriate HRP-conjugated secondary antibody (Cell Signaling Technology,
630 Danvers, MA, USA) at a 1:1,000 dilution. Immunoreactive bands were visualized using
631 Luminol chemiluminescent HRP substrate (Millipore, Burlington, MA, USA) and analyzed
632 with ImageQuant TL Software (GE Healthcare, Buckinghamshire, UK).

633

634 **Analysis of the LPS content of PAH/TPP nanoparticles**

635 The HEK-hTLR4-reporter cell line was maintained in DMEM containing 10% FBS,
636 100U/mL penicillin and 100µg/mL streptomycin at 37°C with 5% CO_2. Thirty thousand
637 cells/well were seeded in 96-well microplates and incubated to 70% confluence. The medium
638 was fully replaced and cells were stimulated ON with different concentrations of LPS,

639 0.5mM PAH, 0.3mM TPP, or 0.5mM PAH/TPP NP. The supernatants were harvested and
640 the secreted embryonic alkaline phosphatase (SEAP) was measured.

641

642 ***In vivo* assessment of adjuvant properties**

643 *Inflammasome characterization:* Male six- to nine-week-old wild-type and KO C57BL/6
644 Nlrp3$^{-/-}$, Casp1/11$^{-/-}$, Casp11$^{-/-}$, Gsdmd$^{-/-}$ and IL-1R$^{-/-}$ mice were purchased from the Federal
645 University of Minas Gerais and maintained under 12h cycles of light/dark. Femur and tibiae
646 were removed for BMDM preparation and for immunization assays. Furthermore, male five-
647 to seven-week-old wild-type Balb/c mice were purchased from the Laboratory of
648 Experimental Animals, School of Veterinary Sciences of the University of La Plata (UNLP),
649 Argentina.

650 Mice (C57BL/6 and Balb/c wild-type mice, and null C57BL/6 mice) were immunized once
651 a week for three consecutive weeks intraperitoneally (IP) with OVA-conjugated PAH/TPP
652 NP (NP-OVA) or OVA adjuvanted with aluminum hydroxide (OVA+Alum). As a control,
653 mice were immunized only with 100µg OVA EndoFit$^{(TM)}$. One week after the last
654 immunization, mice were bled and sacrificed for the immune response analysis.

655 *Humoral response assessment:* OVA-specific antibodies were measured by indirect ELISA
656 in different biological samples. Briefly, MaxiSorp plates (NUNC, Roskilde, Denmark) were
657 coated with 1µg/mL OVA, 5mM PAH or 5mM NP in carbonate-bicarbonate buffer, pH=9.6.
658 Coated plates were blocked with 5% equine serum in saline for 1h at 37°C, and subsequently
659 incubated with sera (1/100) for 1h at 37°C. Bound immunoglobulins were detected with anti-
660 mouse IgG-HRP (Biorad, Hercules, CA, USA), anti- mouse IgG1-HRP, anti-mouse IgG2a-

661 HRP (BD Biosciences, Franklin Lakes, NJ, USA) or anti-mouse IgA-HRP (Thermo Fisher
662 Scientific, Waltham, MA, USA). The reaction was developed with TMB (Sigma-Aldrich, St.
663 Louis, MO, USA) and stopped with 2M H_2SO_4. OD was measured at 450 nm with Varioskan
664 Lux (Thermo Fisher Scientific).

665 *Assessment of secreted cytokine from stimulated splenocytes:* Spleen cell suspensions were
666 prepared in RPMI-1640 supplemented with 10% FBS, 10U/mL penicillin and 10mg/mL
667 streptomycin, seeded ($4x10^6$ cells/mL) in culture plates and cultured for 72h at 37°C under
668 controlled atmosphere. Cells were recalled with 10µg/mL OVA, and supernatants were
669 harvested for mIFN-γ, mIL-5 and mIL-13 quantification by ELISA, using commercially
670 available kits (R&D Systems, Minneapolis, MN, USA) and following the manufacturer´s
671 instructions.

672 Cytokines were also assessed by intracytoplasmic flow cytometry in spleen cells.
673 Splenocytes were incubated with brefeldin A (BD Biosciences, Franklin Lakes, NJ, USA)
674 for the last 4h of culture and stained with anti-CD4 (PerCP-Cy5.5) anti-CD8 (APC)
675 monoclonal Ab (Thermo Fisher Scientific, Waltham, MA, USA). Cells were fixed,
676 permeabilized, and stained with an anti-mouse IFN-γ (FITC) (Thermo Fisher Scientific,
677 Waltham, MA, USA). Sample acquisition was performed with a FACS Aria Fusion
678 cytometer, and data were analyzed using the FlowJo software.

679 *Ethics:* All experimental protocols were conducted in strict agreement with international
680 ethical standards for animal experimentation (Helsinki Declaration and its amendments,
681 Amsterdam Protocol of Welfare and Animal Protection and National Institutes of Health,
682 USA NIH, guidelines: Guide for the Care and Use of Laboratory Animals). Anesthetized

683 mice (isoflurane 5%) were killed by cervical dislocation by experienced research personnel,
684 who performed it humanely and effectively. All efforts were made to alleviate suffering
685 during the whole experiment. All protocols were approved by the Institutional Committee
686 for the Care and Use of Laboratory Animals of the School of Sciences (University of La
687 Plata) (Protocol Number: 006-37-21).
688

689 **Statistical analysis**

690 All experiments were repeated at least twice with consistent outcomes. Flow cytometry data
691 were analyzed using FlowJo X, images obtained by microscopy were analyzed using ImageJ.
692 Graphs and data analysis were performed using GraphPad Prism8. Statistical analyses were
693 carried out using one- or two-way ANOVA, followed by the Tukey test to discern significant
694 differences among measurements from different experimental groups or by the t-Student test
695 when applicable. Quantitative data are expressed as mean ± SEM, and statistical significance
696 was defined as $p<0.05$.

697

698

CONFLICT OF INTEREST

None of the authors has a financial, commercial or personal relationship that could inappropriately influence or bias the content of the paper.

AUTHOR CONTRIBUTIONS *GPR* Conceptualization, Data curation, Formal analysis, Investigation, Methodology, Visualization, Writing – original draft, Writing – review & editing**.** *RCS* Data curation, Methodology. *CC* Data curation, Formal analysis, Investigation, Methodology**.** *DSB* Data curation, Formal analysis, Investigation, Methodology**.** *EA* Data curation, Methodology**.** *SEH* Data curation, Methodology, Writing – original draft, Writing – review & editing**.** *MLA* Data curation, Methodology**.** MLC Data curation, Methodology, Writing – review & editing. WAM Data curation, Methodology, Writing – review & editing. IK Formal analysis, Methodology, Writing-review & editing. AT Formal analysis, Methodology, Writing-review & editing. *SCO* Supervision, Visualization, Writing – original draft, Writing – review & editing**.** *OA* Supervision, Visualization, Writing – original draft, Writing – review & editing**.** *PLS* Conceptualization, Data curation, Formal analysis, Funding acquisition, Investigation, Methodology, Supervision, Visualization, Writing – original draft, Writing – review & editing**.** *GHD* Conceptualization, Formal analysis, Funding acquisition, Investigation, Supervision, Visualization, Writing – original draft, Writing – review & editing.

FUNDINGS

This research was supported by grants from the Universidad Nacional de La Plata [UNLP, grant No. 11/X695] and the Agencia Nacional de Promoción Científica y Tecnológica [ANPCyT, grant No. PICT 2019-0368 and 2020-3166] to PLS and GHD.

ACKNOWLEDGMENTSSHE, MLA, MLC, WAM, AT, OA, PLS and GHD are researchers of CONICET; RCS and SCO are researchers of *Federal University of Minas Gerais; GPR, DSB and EA are* fellows of CONICET; CC and IK are fellows of ANPCyT.

729 **REFERENCES**

730 (1) Rodrigues, C. M. C.; Plotkin, S. A. Impact of Vaccines; Health, Economic and
731 Social Perspectives. *Front. Microbiol.* **2020**, *11*.
732 https://doi.org/10.3389/fmicb.2020.01526.

733 (2) Malonis, R. J.; Lai, J. R.; Vergnolle, O. Peptide-Based Vaccines: Current Progress
734 and Future Challenges. *Chem. Rev.* **2020**, *120* (6), 3210–3229.
735 https://doi.org/10.1021/acs.chemrev.9b00472.

736 (3) Gause, K. T.; Wheatley, A. K.; Cui, J.; Yan, Y.; Kent, S. J.; Caruso, F.
737 Immunological Principles Guiding the Rational Design of Particles for Vaccine
738 Delivery. *ACS Nano* **2017**, *11* (1), 54–68. https://doi.org/10.1021/acsnano.6b07343.

739 (4) Zhao, T.; Cai, Y.; Jiang, Y.; He, X.; Wei, Y.; Yu, Y.; Tian, X. Vaccine Adjuvants:
740 Mechanisms and Platforms. *Signal Transduct. Target. Ther.* **2023**, *8* (1), 283.
741 https://doi.org/10.1038/s41392-023-01557-7.

742 (5) Shi, S.; Zhu, H.; Xia, X.; Liang, Z.; Ma, X.; Sun, B. Vaccine Adjuvants:
743 Understanding the Structure and Mechanism of Adjuvanticity. *Vaccine* **2019**, *37*
744 (24), 3167–3178. https://doi.org/10.1016/j.vaccine.2019.04.055.

745 (6) Pulendran, B.; S. Arunachalam, P.; O'Hagan, D. T. Emerging Concepts in the
746 Science of Vaccine Adjuvants. *Nat. Rev. Drug Discov.* **2021**, *20* (6), 454–475.
747 https://doi.org/10.1038/s41573-021-00163-y.

748 (7) Zhao, L.; Skwarczynski, M.; Toth, I. Polyelectrolyte-Based Platforms for the
749 Delivery of Peptides and Proteins. *ACS Biomater. Sci. Eng.* **2019**, *5* (10), 4937–

750 4950. https://doi.org/10.1021/acsbiomaterials.9b01135.

751 (8) Chen, H.; Zhu, Z.; Lv, K.; Qi, Y.; Si, X.; Ma, S.; Song, W.; Chen, X. Uniform
752 Polymeric Nanovaccine Platform for Improving the Availability and Efficacy of
753 Neoantigen Peptides. *Nano Lett.* **2024**, *24* (33), 10114–10123.
754 https://doi.org/10.1021/acs.nanolett.4c02196.

755 (9) Kim, H. Y.; Kang, M.; Choo, Y. W.; Go, S.; Kwon, S. P.; Song, S. Y.; Sohn, H. S.;
756 Hong, J.; Kim, B.-S. Immunomodulatory Lipocomplex Functionalized with
757 Photosensitizer-Embedded Cancer Cell Membrane Inhibits Tumor Growth and
758 Metastasis. *Nano Lett.* **2019**, *19* (8), 5185–5193.
759 https://doi.org/10.1021/acs.nanolett.9b01571.

760 (10) Walls, A. C.; Fiala, B.; Schäfer, A.; Wrenn, S.; Pham, M. N.; Murphy, M.; Tse, L.
761 V.; Shehata, L.; O'Connor, M. A.; Chen, C.; Navarro, M. J.; Miranda, M. C.; Pettie,
762 D.; Ravichandran, R.; Kraft, J. C.; Ogohara, C.; Palser, A.; Chalk, S.; Lee, E. C.;
763 Guerriero, K.; Kepl, E.; Chow, C. M.; Sydeman, C.; Hodge, E. A.; Brown, B.;
764 Fuller, J. T.; Dinnon, K. H.; Gralinski, L. E.; Leist, S. R.; Gully, K. L.; Lewis, T. B.;
765 Guttman, M.; Chu, H. Y.; Lee, K. K.; Fuller, D. H.; Baric, R. S.; Kellam, P.; Carter,
766 L.; Pepper, M.; Sheahan, T. P.; Veesler, D.; King, N. P. Elicitation of Potent
767 Neutralizing Antibody Responses by Designed Protein Nanoparticle Vaccines for
768 SARS-CoV-2. *Cell* **2020**, *183* (5), 1367-1382.e17.
769 https://doi.org/10.1016/j.cell.2020.10.043.

770 (11) Arunachalam, P. S.; Walls, A. C.; Golden, N.; Atyeo, C.; Fischinger, S.; Li, C.; Aye,
771 P.; Navarro, M. J.; Lai, L.; Edara, V. V.; Röltgen, K.; Rogers, K.; Shirreff, L.;

Ferrell, D. E.; Wrenn, S.; Pettie, D.; Kraft, J. C.; Miranda, M. C.; Kepl, E.; Sydeman, C.; Brunette, N.; Murphy, M.; Fiala, B.; Carter, L.; White, A. G.; Trisal, M.; Hsieh, C. L.; Russell-Lodrigue, K.; Monjure, C.; Dufour, J.; Spencer, S.; Doyle-Meyers, L.; Bohm, R. P.; Maness, N. J.; Roy, C.; Plante, J. A.; Plante, K. S.; Zhu, A.; Gorman, M. J.; Shin, S.; Shen, X.; Fontenot, J.; Gupta, S.; O'Hagan, D. T.; Van Der Most, R.; Rappuoli, R.; Coffman, R. L.; Novack, D.; McLellan, J. S.; Subramaniam, S.; Montefiori, D.; Boyd, S. D.; Flynn, J. A. L.; Alter, G.; Villinger, F.; Kleanthous, H.; Rappaport, J.; Suthar, M. S.; King, N. P.; Veesler, D.; Pulendran, B. Adjuvanting a Subunit COVID-19 Vaccine to Induce Protective Immunity. *Nature* **2021**, *594* (7862), 253–258. https://doi.org/10.1038/s41586-021-03530-2.

(12) Dalvie, N. C.; Rodriguez-Aponte, S. A.; Hartwell, B. L.; Tostanoski, L. H.; Biedermann, A. M.; Crowell, L. E.; Kaur, K.; Kumru, O. S.; Carter, L.; Yu, J.; Chang, A.; McMahan, K.; Courant, T.; Lebas, C.; Lemnios, A. A.; Rodrigues, K. A.; Silva, M.; Johnston, R. S.; Naranjo, C. A.; Tracey, M. K.; Brady, J. R.; Whittaker, C. A.; Yun, D.; Brunette, N.; Wang, J. Y.; Walkey, C.; Fiala, B.; Kar, S.; Porto, M.; Lok, M.; Andersen, H.; Lewis, M. G.; Love, K. R.; Camp, D. L.; Silverman, J. M.; Kleanthous, H.; Joshi, S. B.; Volkin, D. B.; Dubois, P. M.; Collin, N.; King, N. P.; Barouch, D. H.; Irvine, D. J.; Love, J. C. Engineered SARS-CoV-2 Receptor Binding Domain Improves Manufacturability in Yeast and Immunogenicity in Mice. *Proc. Natl. Acad. Sci. U. S. A.* **2021**, *118* (38). https://doi.org/10.1073/pnas.2106845118.

(13) Ren, H.; Jia, W.; Xie, Y.; Yu, M.; Chen, Y. Adjuvant Physiochemistry and Advanced Nanotechnology for Vaccine Development. *Chem. Soc. Rev.* **2023**, *52*

795 (15), 5172–5254. https://doi.org/10.1039/D2CS00848C.

796 (14) He, X.; Zhou, S.; Huang, W.-C.; Seffouh, A.; Mabrouk, M. T.; Morgan, M. T.;
797 Ortega, J.; Abrams, S. I.; Lovell, J. F. A Potent Cancer Vaccine Adjuvant System for
798 Particleization of Short, Synthetic CD8 + T Cell Epitopes. *ACS Nano* **2021**, *15* (3),
799 4357–4371. https://doi.org/10.1021/acsnano.0c07680.

800 (15) Shao, S.; Cao, Z.; Xiao, Z.; Yu, B.; Hu, L.; Du, X.-J.; Yang, X. Programming of in
801 Situ Tumor Vaccines via Supramolecular Nanodrug/Hydrogel Composite and
802 Deformable Nanoadjuvant for Cancer Immunotherapy. *Nano Lett.* **2024**, *24* (29),
803 9017–9026. https://doi.org/10.1021/acs.nanolett.4c02113.

804 (16) Shetty, S.; Alvarado, P. C.; Pettie, D.; Collier, J. H. Next-Generation Vaccine
805 Development with Nanomaterials: Recent Advances, Possibilities, and Challenges.
806 *Annu. Rev. Biomed. Eng.* **2024**, *26* (1), 273–306. https://doi.org/10.1146/annurev-
807 bioeng-110122-124359.

808 (17) Chauhan, G.; Madou, M. J.; Kalra, S.; Chopra, V.; Ghosh, D.; Martinez-Chapa, S. O.
809 Nanotechnology for COVID-19: Therapeutics and Vaccine Research. *ACS Nano*
810 **2020**, *14* (7), 7760–7782. https://doi.org/10.1021/acsnano.0c04006.

811 (18) Xia, H.; Qin, M.; Wang, Z.; Wang, Y.; Chen, B.; Wan, F.; Tang, M.; Pan, X.; Yang,
812 Y.; Liu, J.; Zhao, R.; Zhang, Q.; Wang, Y. A PH-/Enzyme-Responsive Nanoparticle
813 Selectively Targets Endosomal Toll-like Receptors to Potentiate Robust Cancer
814 Vaccination. *Nano Lett.* **2022**, *22* (7), 2978–2987.
815 https://doi.org/10.1021/acs.nanolett.2c00185.

816 (19) Boraschi, D.; Italiani, P.; Palomba, R.; Decuzzi, P.; Duschl, A.; Fadeel, B.;

817 Moghimi, S. M. Nanoparticles and Innate Immunity: New Perspectives on Host
818 Defence. *Semin. Immunol.* **2017**, *34*, 33–51.
819 https://doi.org/10.1016/j.smim.2017.08.013.

820 (20) Genito, C. J.; Batty, C. J.; Bachelder, E. M.; Ainslie, K. M. Considerations for Size,
821 Surface Charge, Polymer Degradation, Co-Delivery, and Manufacturability in the
822 Development of Polymeric Particle Vaccines for Infectious Diseases. *Adv.*
823 *NanoBiomed Res.* **2021**, *1* (3), 2000041. https://doi.org/10.1002/anbr.202000041.

824 (21) Fadeel, B. Clear and Present Danger ? Engineered Nanoparticles and the Immune
825 System. **2012**, No. June, 1–9. https://doi.org/10.4414/smw.2012.13609.

826 (22) Kawai, T.; Akira, S. The Role of Pattern-Recognition Receptors in Innate Immunity:
827 Update on Toll-like Receptors. *Nat. Immunol.* **2010**, *11* (5), 373–384.
828 https://doi.org/10.1038/ni.1863.

829 (23) Iwasaki, A.; Medzhitov, R. Control of Adaptive Immunity by the Innate Immune
830 System. *Nat. Immunol.* **2015**, *16* (4), 343–353. https://doi.org/10.1038/ni.3123.

831 (24) Serrano-Puebla, A.; Boya, P. Lysosomal Membrane Permeabilization in Cell Death:
832 New Evidence and Implications for Health and Disease. *Ann. N. Y. Acad. Sci.* **2016**,
833 *1371* (1), 30–44. https://doi.org/10.1111/nyas.12966.

834 (25) Zhivaki, D.; Borriello, F.; Chow, O. A.; Doran, B.; Fleming, I.; Theisen, D. J.; Pallis,
835 P.; Shalek, A. K.; Sokol, C. L.; Zanoni, I.; Kagan, J. C. Inflammasomes within
836 Hyperactive Murine Dendritic Cells Stimulate Long-Lived T Cell-Mediated Anti-
837 Tumor Immunity. *Cell Rep.* **2020**, *33* (7), 108381.
838 https://doi.org/10.1016/j.celrep.2020.108381.

839 (26) Evavold, C. L.; Ruan, J.; Tan, Y.; Xia, S.; Wu, H.; Kagan, J. C. The Pore-Forming
840 Protein Gasdermin D Regulates Interleukin-1 Secretion from Living Macrophages.
841 *Immunity* **2018**, *48* (1), 35-44.e6. https://doi.org/10.1016/j.immuni.2017.11.013.

842 (27) Monteleone, M.; Stanley, A. C.; Chen, K. W.; Brown, D. L.; Bezbradica, J. S.; von
843 Pein, J. B.; Holley, C. L.; Boucher, D.; Shakespear, M. R.; Kapetanovic, R.; Rolfes,
844 V.; Sweet, M. J.; Stow, J. L.; Schroder, K. Interleukin-1β Maturation Triggers Its
845 Relocation to the Plasma Membrane for Gasdermin-D-Dependent and -Independent
846 Secretion. *Cell Rep.* **2018**, *24* (6), 1425–1433.
847 https://doi.org/10.1016/j.celrep.2018.07.027.

848 (28) Saeki, A.; Tsuchiya, K.; Suda, T.; Into, T.; Hasebe, A.; Suzuki, T.; Shibata, K.
849 ichiro. Gasdermin D-Independent Release of Interleukin-1β by Living Macrophages
850 in Response to Mycoplasmal Lipoproteins and Lipopeptides. *Immunology* **2020**, *161*
851 (2), 114–122. https://doi.org/10.1111/imm.13230.

852 (29) Brubaker, S. W.; Bonham, K. S.; Zanoni, I.; Kagan, J. C. *Innate Immune Pattern*
853 *Recognition : A Cell Biological Perspective*; 2015. https://doi.org/10.1146/annurev-
854 immunol-032414-112240.

855 (30) Qu, Y.; Franchi, L.; Nunez, G.; Dubyak, G. R. Nonclassical IL-1β Secretion
856 Stimulated by P2X7 Receptors Is Dependent on In?Ammasome Activation and
857 Correlated with Exosome Release in Murine Macrophages. **2015**.
858 https://doi.org/10.4049/jimmunol.179.3.1913.

859 (31) Abu Khweek, A.; Amer, A. O. Pyroptotic and Non-Pyroptotic Effector Functions of
860 Caspase-11. *Immunol. Rev.* **2020**, *297* (1), 39–52. https://doi.org/10.1111/imr.12910.

861 (32) Kayagaki, N.; Warming, S.; Lamkanfi, M.; Walle, L. Vande; Louie, S.; Dong, J.;
862 Newton, K.; Qu, Y.; Liu, J.; Heldens, S.; Zhang, J.; Lee, W. P.; Roose-Girma, M.;
863 Dixit, V. M. Non-Canonical Inflammasome Activation Targets Caspase-11. *Nature*
864 **2011**, *479* (7371), 117–121. https://doi.org/10.1038/nature10558.

865 (33) Desai, D. N.; Mahal, A.; Varshney, R.; Obaidullah, A. J.; Gupta, B.; Mohanty, P.;
866 Pattnaik, P.; Mohapatra, N. C.; Mishra, S.; Kandi, V.; Rabaan, A. A.; Mohapatra, R.
867 K. Nanoadjuvants: Promising Bioinspired and Biomimetic Approaches in Vaccine
868 Innovation. *ACS Omega* **2023**, *8* (31), 27953–27968.
869 https://doi.org/10.1021/acsomega.3c02030.

870 (34) Tenchov, R.; Bird, R.; Curtze, A. E.; Zhou, Q. Lipid Nanoparticles─From
871 Liposomes to MRNA Vaccine Delivery, a Landscape of Research Diversity and
872 Advancement. *ACS Nano* **2021**, *15* (11), 16982–17015.
873 https://doi.org/10.1021/acsnano.1c04996.

874 (35) Gu, P.; Wusiman, A.; Zhang, Y.; Liu, Z.; Bo, R.; Hu, Y.; Liu, J.; Wang, D. Rational
875 Design of PLGA Nanoparticle Vaccine Delivery Systems To Improve Immune
876 Responses. *Mol. Pharm.* **2019**, *16* (12), 5000–5012.
877 https://doi.org/10.1021/acs.molpharmaceut.9b00860.

878 (36) Ou, B. S.; Baillet, J.; Filsinger Interrante, M. V.; Adamska, J. Z.; Zhou, X.; Saouaf,
879 O. M.; Yan, J.; Klich, J. H.; Jons, C. K.; Meany, E. L.; Valdez, A. S.; Carter, L.;
880 Pulendran, B.; King, N. P.; Appel, E. A. Saponin Nanoparticle Adjuvants
881 Incorporating Toll-like Receptor Agonists Drive Distinct Immune Signatures and
882 Potent Vaccine Responses. *Sci. Adv.* **2024**, *10* (32).

883 https://doi.org/10.1126/sciadv.adn7187.

884 (37) Rose, F.; Wern, J. E.; Gavins, F.; Andersen, P.; Follmann, F.; Foged, C. A Strong
885 Adjuvant Based on Glycol-Chitosan-Coated Lipid-Polymer Hybrid Nanoparticles
886 Potentiates Mucosal Immune Responses against the Recombinant Chlamydia
887 Trachomatis Fusion Antigen CTH522. *J. Control. Release* **2018**, *271*, 88–97.
888 https://doi.org/10.1016/j.jconrel.2017.12.003.

889 (38) Lei, H.; Alu, A.; Yang, J.; Ren, W.; He, C.; Lan, T.; He, X.; Yang, L.; Li, J.; Wang,
890 Z.; Song, X.; Wang, W.; Lu, G.; Wei, X. Intranasal Administration of a
891 Recombinant RBD Vaccine Induces Long-Term Immunity against Omicron-
892 Included SARS-CoV-2 Variants. *Signal Transduct. Target. Ther.* **2022**, *7* (1), 159.
893 https://doi.org/10.1038/s41392-022-01002-1.

894 (39) Han, H. D.; Byeon, Y.; Jang, J.-H.; Jeon, H. N.; Kim, G. H.; Kim, M. G.; Pack, C.-
895 G.; Kang, T. H.; Jung, I. D.; Lim, Y. T.; Lee, Y. J.; Lee, J.-W.; Shin, B. C.; Ahn, H.
896 J.; Sood, A. K.; Park, Y.-M. In Vivo Stepwise Immunomodulation Using Chitosan
897 Nanoparticles as a Platform Nanotechnology for Cancer Immunotherapy. *Sci. Rep.*
898 **2016**, *6* (1), 38348. https://doi.org/10.1038/srep38348.

899 (40) Han, Y.; Duan, Q.; Li, Y.; Tian, J. In Vitro and in Vivo Investigation of Chitosan–
900 Polylysine Polymeric Nanoparticles for Ovalbumin and CpG Co-Delivery. *RSC Adv.*
901 **2017**, *7* (63), 39962–39969. https://doi.org/10.1039/C7RA06450K.

902 (41) Lei, H.; Alu, A.; Yang, J.; He, C.; Hong, W.; Cheng, Z.; Yang, L.; Li, J.; Wang, Z.;
903 Wang, W.; Lu, G.; Wei, X. Cationic Nanocarriers as Potent Adjuvants for
904 Recombinant S-RBD Vaccine of SARS-CoV-2. *Signal Transduct. Target. Ther.*

905 **2020**, *5* (1), 291. https://doi.org/10.1038/s41392-020-00434-x.

906 (42) Brunot, C.; Ponsonnet, L.; Lagneau, C.; Farge, P.; Picart, C.; Grosgogeat, B.
907 Cytotoxicity of Polyethyleneimine (PEI), Precursor Base Layer of Polyelectrolyte
908 Multilayer Films. *Biomaterials* **2007**, *28* (4), 632–640.
909 https://doi.org/10.1016/j.biomaterials.2006.09.026.

910 (43) Sanità, G.; Carrese, B.; Lamberti, A. Nanoparticle Surface Functionalization: How to
911 Improve Biocompatibility and Cellular Internalization. *Front. Mol. Biosci.* **2020**, *7*,
912 587012. https://doi.org/10.3389/fmolb.2020.587012.

913 (44) Apuzzo, E.; Agazzi, M.; Herrera, S. E.; Picco, A.; Rizzo, G.; Chavero, C.; Bianchi,
914 D.; Smaldini, P.; Cortez, M. L.; Marmisollé, W. A.; Padula, G.; Seoane, A.; Alomar,
915 M. L.; Denofrio, M. P.; Docena, G.; Azzaroni, O. Poly(Allylamine)-
916 Tripolyphosphate Ionic Assemblies as Nanocarriers: Friend or Foe? *ACS Appl. Bio*
917 *Mater.* **2023**, *6* (11), 4714–4727. https://doi.org/10.1021/acsabm.3c00489.

918 (45) E. Apuzzo, M. Agazzi, S. Herrera, A. Picco, G. Rizzo, C. Chavero, D. Bianchi, P.
919 Smaldini, L. Cortez, W. Marmisollé, G. Padula, A. Seoane, M. Alomar, M.
920 Denofrio, G. Docena, O. A. Poly (Allylamine) -Tripolyphosphate Ionic Assemblies
921 as Nanocarriers : Friend or Foe? **2023**. https://doi.org/10.1021/acsabm.3c00489.

922 (46) Bourque, J.; Hawiger, D. *Immunomodulatory Bonds of the Partnership between*
923 *Dendritic Cells and T Cells*; 2018; Vol. 38.
924 https://doi.org/10.1615/CritRevImmunol.2018026790.

925 (47) Reddy, S. T.; Swartz, M. A.; Hubbell, J. A. Targeting Dendritic Cells with
926 Biomaterials: Developing the next Generation of Vaccines. *Trends Immunol.* **2006**,

927 *27* (12), 573–579. https://doi.org/10.1016/j.it.2006.10.005.

928 (48) Babensee, J. E. Interaction of Dendritic Cells with Biomaterials. *Semin. Immunol.*
929 **2008**, *20* (2), 101–108. https://doi.org/10.1016/j.smim.2007.10.013.

930 (49) Herrera, S. E.; Agazzi, M. L.; Apuzzo, E.; Cortez, M. L.; Marmisollé, W. A.;
931 Tagliazucchi, M.; Azzaroni, O. Polyelectrolyte-Multivalent Molecule Complexes:
932 Physicochemical Properties and Applications. *Soft Matter* **2023**, *19* (11), 2013–2041.
933 https://doi.org/10.1039/D2SM01507B.

934 (50) Coria-Oriundo, L. L.; Debais, G.; Apuzzo, E.; Herrera, S. E.; Ceolín, M.; Azzaroni,
935 O.; Battaglini, F.; Tagliazucchi, M. Phase Behavior and Electrochemical Properties
936 of Highly Asymmetric Redox Coacervates. *J. Phys. Chem. B* **2023**, *127* (35), 7636–
937 7647. https://doi.org/10.1021/acs.jpcb.3c03680.

938 (51) Cullen, S. P.; Kearney, C. J.; Clancy, D. M.; Martin, S. J. Diverse Activators of the
939 NLRP3 Inflammasome Promote IL-1β Secretion by Triggering Necrosis. *Cell Rep.*
940 **2015**, *11* (10), 1535–1548. https://doi.org/10.1016/j.celrep.2015.05.003.

941 (52) Chan, A. H.; Schroder, K. Inflammasome Signaling and Regulation of Interleukin-1
942 Family Cytokines. *J. Exp. Med.* **2020**, *217* (1), 1–10.
943 https://doi.org/10.1084/jem_20190314.

944 (53) Hoss, F.; Rodriguez-Alcazar, J. F.; Latz, E. Assembly and Regulation of ASC
945 Specks. *Cell. Mol. Life Sci.* **2017**, *74* (7), 1211–1229.
946 https://doi.org/10.1007/s00018-016-2396-6.

947 (54) Sester, D. P.; Thygesen, S. J.; Sagulenko, V.; Vajjhala, P. R.; Cridland, J. A.; Vitak,
948 N.; Chen, K. W.; Osborne, G. W.; Schroder, K.; Stacey, K. J. A Novel Flow

949 Cytometric Method To Assess Inflammasome Formation. *J. Immunol.* **2015**, *194* (1),
950 455–462. https://doi.org/10.4049/jimmunol.1401110.

951 (55) Iula, L.; Keitelman, I. A.; Sabbione, F.; Fuentes, F.; Guzman, M.; Galletti, J. G.;
952 Gerber, P. P.; Ostrowski, M.; Geffner, J. R.; Jancic, C. C.; Trevani, A. S. Autophagy
953 Mediates Interleukin-1β Secretion in Human Neutrophils. *Front. Immunol.* **2018**, *9*
954 (FEB), 1–14. https://doi.org/10.3389/fimmu.2018.00269.

955 (56) Dupont, N.; Jiang, S.; Pilli, M.; Ornatowski, W.; Bhattacharya, D.; Deretic, V.
956 Autophagy-Based Unconventional Secretory Pathway for Extracellular Delivery of
957 IL-1β. *EMBO J.* **2011**, *30* (23), 4701–4711. https://doi.org/10.1038/emboj.2011.398.

958 (57) Kwissa, M.; Kasturi, S. P.; Pulendran, B. The Science of Adjuvants. *Expert Rev.*
959 *Vaccines* **2007**, *6* (5), 673–684. https://doi.org/10.1586/14760584.6.5.673.

960 (58) Hornung, V.; Bauernfeind, F.; Halle, A.; Samstad, E. O.; Kono, H.; Rock, K. L.;
961 Fitzgerald, K. A.; Latz, E. Silica Crystals and Aluminum Salts Activate the NALP3
962 Inflammasome through Phagosomal Destabilization. *Nat. Immunol.* **2008**, *9* (8),
963 847–856. https://doi.org/10.1038/ni.1631.

964 (59) Ma, L.; Han, Z.; Yin, H.; Tian, J.; Zhang, J.; Li, N.; Zhang, L. Characterization of
965 Cathepsin B in Mediating Silica Nanoparticle-Induced Macrophage Pyroptosis via
966 an NLRP3-Dependent Manner. **2022**, No. August, 4537–4545.

967 (60) Chevriaux, A.; Pilot, T.; Derangère, V.; Simonin, H.; Martine, P.; Chalmin, F.;
968 Ghiringhelli, F.; Rébé, C. Cathepsin B Is Required for NLRP3 Inflammasome
969 Activation in Macrophages, Through NLRP3 Interaction. *Front. Cell Dev. Biol.*
970 **2020**, *8* (March), 1–8. https://doi.org/10.3389/fcell.2020.00167.

971 (61) Sahoo, M.; Ceballos-Olvera, I.; Del Barrio, L.; Re, F. Role of the Inflammasome, IL-
972 1β, and IL-18 in Bacterial Infections. *ScientificWorldJournal.* **2011**, *11*, 2037–2050.
973 https://doi.org/10.1100/2011/212680.

974 (62) Baroja-Mazo, A.; Compan, V.; Martín-Sánchez, F.; Tapia-Abellán, A.; Couillin, I.;
975 Pelegrín, P. Early Endosome Autoantigen 1 Regulates IL-1β Release upon Caspase-
976 1 Activation Independently of Gasdermin D Membrane Permeabilization. *Sci. Rep.*
977 **2019**, *9* (1), 1–10. https://doi.org/10.1038/s41598-019-42298-4.

978 (63) Ponpuak, M.; Mandell, M. A.; Kimura, T.; Chauhan, S.; Cleyrat, C.; Deretic, V.
979 Secretory Autophagy. *Curr. Opin. Cell Biol.* **2015**, *35* (Figure 1), 106–116.
980 https://doi.org/10.1016/j.ceb.2015.04.016.

981 (64) Deretic, V. Autophagy in Inflammation, Infection, and Immunometabolism.
982 *Immunity* **2021**, *54* (3), 437–453. https://doi.org/10.1016/j.immuni.2021.01.018.

983 (65) Kimura, T.; Jia, J.; Kumar, S.; Choi, S. W.; Gu, Y.; Mudd, M.; Dupont, N.; Jiang, S.;
984 Peters, R.; Farzam, F.; Jain, A.; Lidke, K. A.; Adams, C. M.; Johansen, T.; Deretic,
985 V. Dedicated SNARE s and Specialized TRIM Cargo Receptors Mediate Secretory
986 Autophagy . *EMBO J.* **2017**, *36* (1), 42–60.
987 https://doi.org/10.15252/embj.201695081.

988 (66) Sweatt,S.K, Gower, B.A, Chieh, A.Y, Liu, Y, Li, L. Crucial Role for the Nalp3
989 Inflammasome in the Immunostimulatory Properties of Aluminium Adjuvants.
990 *Physiol. Behav.* **2016**, *176* (1), 139–148.
991 https://doi.org/10.1038/nature06939.Crucial.

992 (67) Daniel E Shumer, Natalie J Nokoff, N. P. S.; Erin C. Dowd, M.D.a, Michael J.

993 Frank, Ph.D.b, Anne Collins, Ph.D.c, James M. Goldd, and Deanna M. Barch, P. D. .
994 T Helper 1 Immunity Requires Complement-Driven NLRP3 Inflammasome Activity
995 in CD4+ T Cells. *Physiol. Behav.* **2017**, *176* (12), 139–148.
996 https://doi.org/10.1126/science.aad1210.T.

997 (68) Wagatsuma, K.; Nakase, H. Contradictory Effects of NLRP3 Inflammasome
998 Regulatory Mechanisms in Colitis. *Int. J. Mol. Sci.* **2020**, *21* (21), 1–24.
999 https://doi.org/10.3390/ijms21218145.

1000 (69) Marty-Roix, R.; Vladimer, G. I.; Pouliot, K.; Weng, D.; Buglione-Corbett, R.; West,
1001 K.; MacMicking, J. D.; Chee, J. D.; Wang, S.; Lu, S.; Lien, E. Identification of QS-
1002 21 as an Inflammasome-Activating Molecular Component of Saponin Adjuvants. *J.*
1003 *Biol. Chem.* **2016**, *291* (3), 1123–1136. https://doi.org/10.1074/jbc.M115.683011.

1004 (70) Kool, M.; Soullié, T.; Van Nimwegen, M.; Willart, M. A. M.; Muskens, F.; Jung, S.;
1005 Hoogsteden, H. C.; Hammad, H.; Lambrecht, B. N. Alum Adjuvant Boosts Adaptive
1006 Immunity by Inducing Uric Acid and Activating Inflammatory Dendritic Cells. *J.*
1007 *Exp. Med.* **2008**, *205* (4), 869–882. https://doi.org/10.1084/jem.20071087.

1008 (71) Content, R. Alum ' s Adjuvant Effect Are Mediated by NLRP3 1. **2014**, *181* (2008),
1009 17–21.

1010 (72) Muñoz-Wolf, N.; Ward, R. W.; Hearnden, C. H.; Sharp, F. A.; Geoghegan, J.;
1011 O'Grady, K.; McEntee, C. P.; Shanahan, K. A.; Guy, C.; Bowie, A. G.; Campbell,
1012 M.; Roces, C. B.; Anderluzzi, G.; Webb, C.; Perrie, Y.; Creagh, E.; Lavelle, E. C.
1013 Non-Canonical Inflammasome Activation Mediates the Adjuvanticity of
1014 Nanoparticles. *Cell Reports Med.* **2023**, *4* (1).

1015 https://doi.org/10.1016/j.xcrm.2022.100899.

1016 (73) Kaplanski, G. Interleukin-18: Biological Properties and Role in Disease
1017 Pathogenesis. *Immunol. Rev.* **2018**, *281* (1), 138–153.
1018 https://doi.org/10.1111/imr.12616.

1019 (74) Lacaille-Dubois, M. A. Updated Insights into the Mechanism of Action and Clinical
1020 Profile of the Immunoadjuvant QS-21: A Review. *Phytomedicine* **2019**, *60* (March),
1021 152905. https://doi.org/10.1016/j.phymed.2019.152905.

1022 (75) Weischenfeldt, J.; Porse, B. Bone Marrow-Derived Macrophages (BMM): Isolation
1023 and Applications. *Cold Spring Harb. Protoc.* **2008**, *2008* (12), pdb.prot5080.
1024 https://doi.org/10.1101/pdb.prot5080.

1025